J. Am. Soc. Mass Spectrom. (2011) 22:731–751
DOI: 10.1007/s13361-011-0083-2

RESEARCH ARTICLE

Dipole-Guided Electron Capture Causes Abnormal Dissociations of Phosphorylated Pentapeptides

Christopher L. Moss,[1] Thomas W. Chung,[1] Jean A. Wyer,[2] Steen Brøndsted Nielsen,[2] Preben Hvelplund,[2] František Tureček[1]

[1]Department of Chemistry, University of Washington, Bagley Hall Box 351700, Seattle, WA 98195-1700, USA
[2]Department of Physics and Astronomy, Aarhus University, Aarhus, Denmark

Abstract

Electron transfer and capture mass spectra of a series of doubly charged ions that were phosphorylated pentapeptides of a tryptic type (pS,A,A,A,R) showed conspicuous differences in dissociations of charge-reduced ions. Electron transfer from both gaseous cesium atoms at 100 keV kinetic energies and fluoranthene anion radicals in an ion trap resulted in the loss of a hydrogen atom, ammonia, and backbone cleavages forming complete series of sequence z ions. Elimination of phosphoric acid was negligible. In contrast, capture of low-energy electrons by doubly charged ions in a Penning ion trap induced loss of a hydrogen atom followed by elimination of phosphoric acid as the dominant dissociation channel. Backbone dissociations of charge-reduced ions also occurred but were accompanied by extensive fragmentation of the primary products. z-Ions that were terminated with a deaminated phosphoserine radical competitively eliminated phosphoric acid and H_2PO_4 radicals. A mechanism is proposed for this novel dissociation on the basis of a computational analysis of reaction pathways and transition states. Electronic structure theory calculations in combination with extensive molecular dynamics mapping of the potential energy surface provided structures for the precursor phosphopeptide dications. Electron attachment produces a multitude of low lying electronic states in charge-reduced ions that determine their reactivity in backbone dissociations and H- atom loss. The predominant loss of H atoms in ECD is explained by a distortion of the Rydberg orbital space by the strong dipolar field of the peptide dication framework. The dipolar field steers the incoming electron to preferentially attach to the positively charged arginine side chain to form guanidinium radicals and trigger their dissociations.

Key words: Electron transfer dissociation, Electron capture dissociation, Phosphopeptides, Sequence ions, Dipole effects, Ion structures, Molecular dynamics calculations, Ab initio calculations

Introduction

Electron-based methods such as electron capture dissociation (ECD) [1] and electron transfer dissociation (ETD) [2, 3], which are collectively referred to as ExD, have been

Received: 15 October 2010
Revised: 6 January 2011
Accepted: 8 January 2011
Published online: 26 February 2011

Christopher L. Moss and Thomas W. Chung contributed equally to this work.

Electronic supplementary material The online version of this article (doi:10.1007/s13361-011-0083-2) contains supplementary material, which is available to authorized users.

Correspondence to: František Tureček; *e-mail:* turecek@chem.washington.edu

shown to be suitable for the analysis of peptides post-translationally modified by phosphorylation [4–12], sulfation [13], or glycosylation [14, 15]. It has been reported that attachment of an electron to multiply protonated phosphopeptides caused backbone fragmentations while preserving the phosphate group in the fragments [4]. This feature has been utilized in studies aimed at the localization of phosphorylated residues in peptides produced by enzymatic digestion of proteins [5–12]. However, it has also been reported that the presence of phosphorylated serine residues hampered backbone dissociations of several synthetic peptides [16]. Electron transfer from alkali metal atoms has been reported recently to induce dissociations yielding sequence fragments from phosphopeptides [17, 18].

The current interpretation of ExD of phosphopeptides is usually based on the general mechanisms dealing with backbone cleavages. These consider a significant weakening of peptide N–C_α bonds as a result of electron or hydrogen atom attachment to the amide carbonyl group [19]. The presumed reactive intermediates in N–C_α bond cleavage are aminoketyl radicals [20] which have low energy barriers to N–C_α bond cleavage [19, 20]. In contrast, the neutral phosphate ester group has a negative electron and hydrogen atom affinity (–37 kJ mol^{-1}), and an H-atom addition faces a substantial barrier in the transition state, e.g., 90 kJ mol^{-1}, as established by ab initio calculations for H-atom adducts to phosphoric acid [21]. Hence, amongst the competitive sites of electron attachment, the neutral phosphate group must be considered to be a poor electron and hydrogen atom acceptor and its elimination is not promoted by electron attachment to the peptide ion.

Whereas both ECD and ETD have been used for the detection of phosphorylated sites in peptides and the pertinent ion fragmentations have been considered analogous [22], there have been reports that pointed out conspicuous differences between ECD and ETD of peptide ions [23]. Therefore, it became of interest to investigate a series of phosphorylated peptides under different conditions of electron attachment. We selected pentapeptides pSAAAR, ApSAAR, AApSAR, and AAApSR as model sequences. These peptides readily form doubly protonated ions by electrospray to be used for ExD studies. In addition, ions derived from these peptides are small enough (74 atoms) to allow us to perform ab initio calculations of structure and energetics and attempt to correlate the computational results with experiments. At the same time, however, pentapeptide ions display intricate patterns of intramolecular hydrogen bonding to provide secondary structure motifs that are representative of those presumed to exist in larger peptide ions [23].

Three series of ExD experiments are reported here. In the first series, doubly charged precursor ions were accelerated to 100 keV kinetic energy and partially discharged by collisions with cesium atoms. These measurements are referred to as electron capture induced dissociation (ECID) [24]. In the second series of measurements, doubly charged precursor ions were partially discharged by ion–ion reactions with fluoranthene molecular anions in an ion trap, corresponding to standard electron transfer dissociation (ETD) [2, 3]. The third series of measurements comprised dissociative recombination of doubly charged precursor ions with free low-energy electrons in a Penning trap, corresponding to electron capture dissociation (ECD) [1]. We wish to show that capture of free electrons in ECD caused dissociations that were dramatically different from those induced by electron transfer in ECID and ETD.

Experimental

Materials

Phosphorylated peptides pSAAAR, ApSAAR, AApSAR, and AAApSR were custom synthesized by GenScript (Piscatway, NJ, USA) and their purities were checked by HPLC to be 98%–99%. The molecular mass and sequence of each was checked by electrospray ionization tandem mass spectrometry. Electrospray from 10 μM solutions in 50/50 methanol-water encompassing 1% acetic acid afforded copious doubly charged phosphopentapeptide ions.

Methods

Electron capture induced dissociation (ECID) mass spectra were obtained on a large-scale sector instrument described previously [24]. Briefly, precursor ions were produced from 1 mM solutions in 50/50/1 water/methanol/acetic acid in an electrospray source floated at 50 kV, and the doubly charged ions were accelerated to 100 keV kinetic energies. The precursor ions were separated by a large scale electromagnet and focused on the entrance slit of the collision chamber filled with Cs vapor. The Cs vapor pressure in the collision cell cannot be measured directly and it was adjusted by temperature control to provide ion beam transmittance corresponding to mostly single-collision conditions. The ion velocity (1.87×10^5 ms^{-1}) and estimated cross section for electron transfer ($\sigma\cong100$ Å^2) give the ion-neutral interaction time as $t=(2/v)(\sigma/\pi)^{1/2}=6\times10^{-15}$ s. Hence, the electron transfer is a nearly vertical process. Charged products of electron transfer were separated by an electrostatic analyzer and detected by ion counting. Multiple scans were collected and averaged to obtain charge-reduced ion counts in the 25,000–100,000 range.

Electron transfer dissociation (ETD) mass spectra were obtained on a Thermo Fisher Scientific (San Jose, CA, USA) LTQ XL linear ion trap instrument equipped with a chemical ionization source for the production of fluoranthene anions as ETD reagent. Precursor $(M+2H)^{2+}$ ions were selected by mass with an isolation width of 5 m/z units so as to accommodate nearest ^{13}C isotopologues. The peptide ions were then reacted with fluoranthene anions for 100 and 200 ms. Multiple-stage tandem MS was performed so as to interrogate z-type ions from ETD. These ETD product ions

and others (e.g., electron-transfer induced product ions resulting from loss of phosphoric acid) were selected by mass and collisionally dissociated with the He bath gas at 20% of rf power.

ECD mass spectra were measured on a Thermo LTQ XL 7 T FT-ICR Ultra mass spectrometer (LTQ-FT). Precursor peptide dications were isolated in the linear trap quadrupole with a 5 *m/z* unit mass selection window, transferred to the ion cyclotron resonance cell, and irradiated by free electrons from an external source. The irradiation pulse width was 300 ms, and the electron emitter bias was set at a nominal potential value of 5 V.

Computations

Our strategy for finding the lowest energy conformations is to first generate a large number of candidate structures in the molecular dynamics regime, then refine the relative energies and re-optimize geometries by semi-empirical and ab initio methods. Molecular dynamics calculations were performed using NAMD [25]. Semiempirical and ab initio calculations were performed using Gaussian 09 [26]. Molecular dynamics force-field parameters have not previously been developed for protonation states that result from electrospray of phosphoserine peptides. Force-field parameters for the singly-protonated phosphoserine species are available [27], but those for doubly-protonated species with neutral phosphate groups have not been previously developed. We combined the results from ref. [27] along with ab initio calculations to develop a set of parameters for the phosphoserine sequences which are given in Table S1 in the Supplementary Material. This parameter set was not intended to be sufficiently characterized to accurately reproduce all thermodynamic properties, but merely accurate enough to generate qualitatively reasonable candidate structures. Other residues were parameterized using established values from the CHARMM force-field [28]. Once the force-field parameters had been determined, replica exchange molecular dynamics (REMD) [29] were performed on each peptide ion sequence. Calculations were run for 10 ns with a step size of 1 fs with 8 temperature replicas from 300 to 800 K. 1000 structures from each replica were selected at regular intervals for a total of 8000 initial candidate structures. Each candidate structure was then optimized at the PM6 level [30]. The PM6 optimized structures were then analyzed for potential hydrogen bonds. Structures with the same hydrogen bonds were grouped together, and the lowest energy structure from each group was taken to form a new list of candidate structures. The single point energy for each candidate structure was calculated at the B3LYP/6-31+G(d,p) [31–33] level of theory, the structures from each sequence with the lowest energy were re-optimized at the same level, and the local minima were confirmed with frequency calculations. The fully optimized geometries of low-energy conformers of $(pSAAAR+2H)^{2+}$($\mathbf{1a^{2+}}$-$\mathbf{1e^{2+}}$), $(ApSAAR+2H)^{2+}$($\mathbf{2a^{2+}}$-$\mathbf{2e^{2+}}$), $(AApSAR+2H)^{2+}$($\mathbf{3a^{2+}}$-$\mathbf{3e^{2+}}$), and $(AAApSR+2H)^{2+}$ ($\mathbf{4a^{2+}}$-$\mathbf{4e^{2+}}$) are given in Cartesian coordinate format as Tables S2–S21 in Supplementary Material. Single point energies were calculated with B3LYP/6-311++G(2d,p) and MP2/6-311++G(2d,p) [34] for each reoptimized structure. The energies calculated from each of these methods were averaged to compensate for known errors in each method [35]. Calculations of radical states began with the optimized dication structures. Selected structures were re-optimized with the charge-reduced electronic configuration at the B3LYP/6-31+G(d,p) level and the local minima were characterized by harmonic frequency calculations. In addition, time dependent density functional theory (TD-DFT) [36] was used to calculate the first 15 excited states of the vertically formed cation-radical configuration at the B3LYP/6-311++G(2d,p) level of theory.

Results

ECID, ETD, and ECD Mass Spectra

Electron transfer from Cs atoms to doubly charged pSAAAR, ApSAAR, AApSAR, and AAApSR ions proceeded with 16%–18% efficiency at 100 keV ion kinetic energies and under single-collision conditions. There were no substantial differences in the electron transfer efficiencies among the isomeric peptide ions. The ECID mass spectra are shown in Figure 1a–d. The spectra display common charge-reduced $(M+2H)^{+\bullet}$ ions at *m/z* 556 and fragments due to loss of H (*m/z* 555), ammonia (*m/z* 539), and a 43 Da neutral fragment (*m/z* 513), presumably $HN{=}C^{\bullet}{-}NH_2$ from the arginine side chain [37]. Another common fragment occurs at *m/z* 441 and corresponds to elimination of phosphoric acid from the *m/z* 539 primary fragment ions. Sequence ions of the z series are observed for all four peptides. ECID of $(pSAAAR+2H)^{2+}$ produced z_1-z_4 ions at *m/z* 159, 230, 301, and 372, respectively (Figure 1a). Those from $(ApSAAR+2H)^{2+}$ appear at *m/z* 159, 230, 301, and 468 (Figure 1b). ECID of $(AApSAR+2H)^{2+}$ gave z_1–z_4 ions at *m/z* 159, 230, 397, and 468, respectively (Figure 1c). Finally, ECID of $(AApSAR+2H)^{2+}$ produced z_1–z_4 ions at z 159, 326, 397, and 468, respectively (Figure 1d). Hence, ECID cleaved all four N–C_α bonds in the peptide ions.

The insets in the Figure 1 spectra indicate different relative abundances of charge reduced $(M+2H)^{+\bullet}$ ions depending on the peptide sequence. After deconvolution of the overlapping *m/z* 555 and 556 peak profiles, one obtains the $(M+2H)^{+\bullet}$ ion abundances as 6%, 11%, 7%, and 12% relative to the sum of charge-reduced ion intensities for pSAAAR, ApSAAR, AApSAR, and AAApSR, respectively. The respective summed relative abundances of the z_1–z_4 ions were 7%, 11%, 9%, and 16% in the same peptide series.

ETD mass spectra of doubly charged pSAAAR, ApSAAR, AApSAR, and AAApSR were obtained at 100- and 200-ms ion–ion interaction time; the 100-ms spectra are shown in Figure 2a–d. In contrast to the ECID spectra,

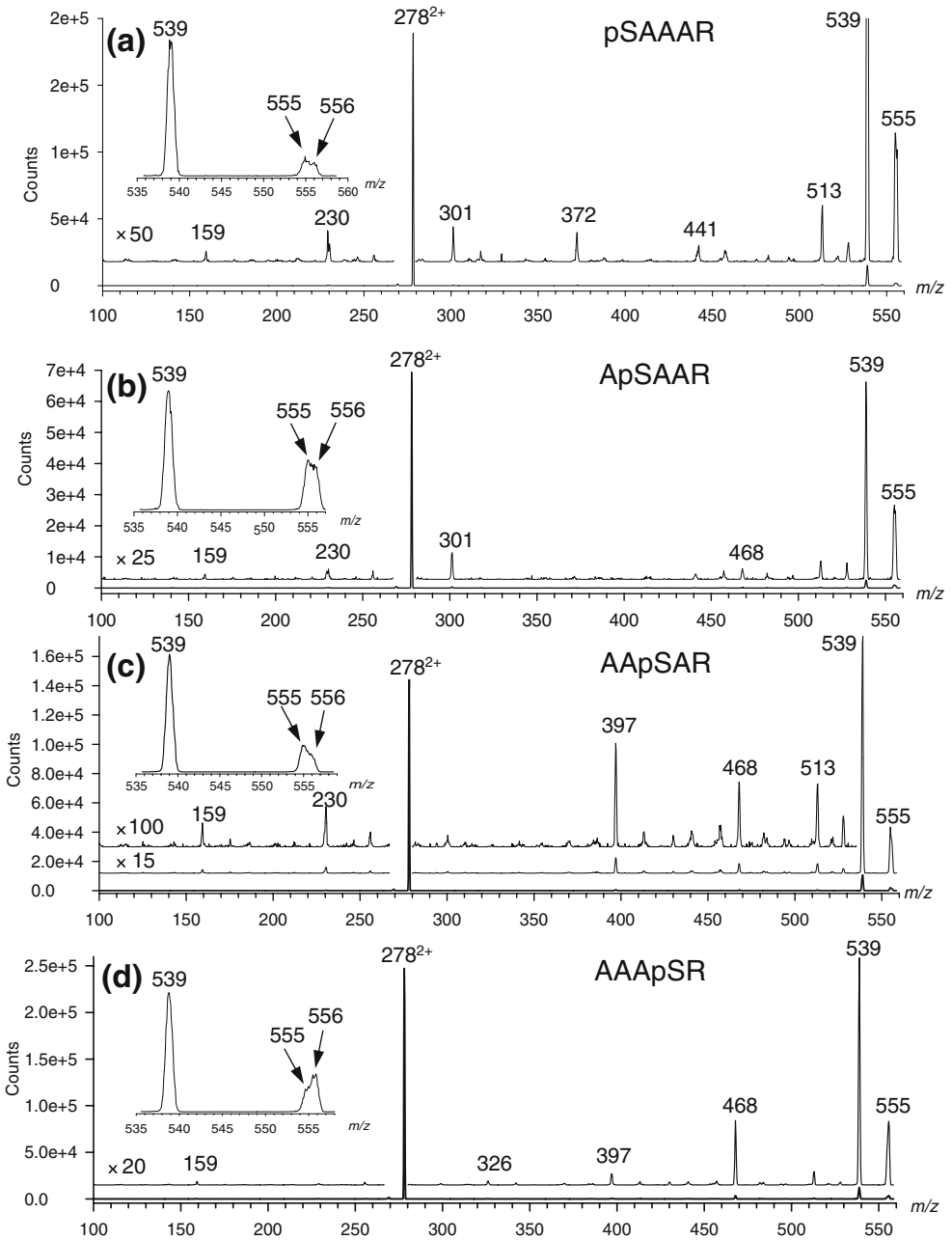

Figure 1. Electron-capture induced dissociation mass spectra of **(a)** $(pSAAAR+2H)^{2+}$, **(b)** $(ApSAAR+2H)^{2+}$, **(c)** $(AApSAR+2H)^{2+}$, and **(d)** $(AAApSR+2H)^{2+}$. Insets show the *m/z* 535–560 region scanned at increased kinetic energy resolution

charge-reduced $(M+2H)^{+\bullet}$ were very weak or absent in the ETD mass spectra. The ion intensities at *m/z* 556, e.g., 3.7% from pSAAAR, can be almost completely accounted by ^{13}C satellites of the abundant $(M + H)^+$ peak (calculated as 3.4%), and likewise for the other peptides. The ETD spectra showed complete series of sequence z fragment ions. The combined z ion relative intensities in the ETD spectra in Figure 2 were 17, 24, 18, and 22% for pSAAAR, ApSAAR, AApSAR, and AAApSR, respectively. Both the combined and individual z_1–z_4 ion relative intensities were remarkably insensitive to the ion–ion interaction time, such that the ETD spectra obtained at 100 and 200 ms ion-ion interaction time showed ion relative intensities within 5% of each other. Of note is also the similarity in the z ion relative intensities in the ECID and ETD spectra. For example, z_3 ions are the most abundant backbone fragments in both ECID and ETD spectra of the ApSAAR and AApSAR ions, and the z_4 ion is most abundant in ETD and ECID of AAApSR. The relative intensities of the z ions are plotted in Figure S1, Supplementary Material.

In contrast to ECID and ETD, the ECD mass spectra of the phosphorylated pentapeptides showed dominant frag-

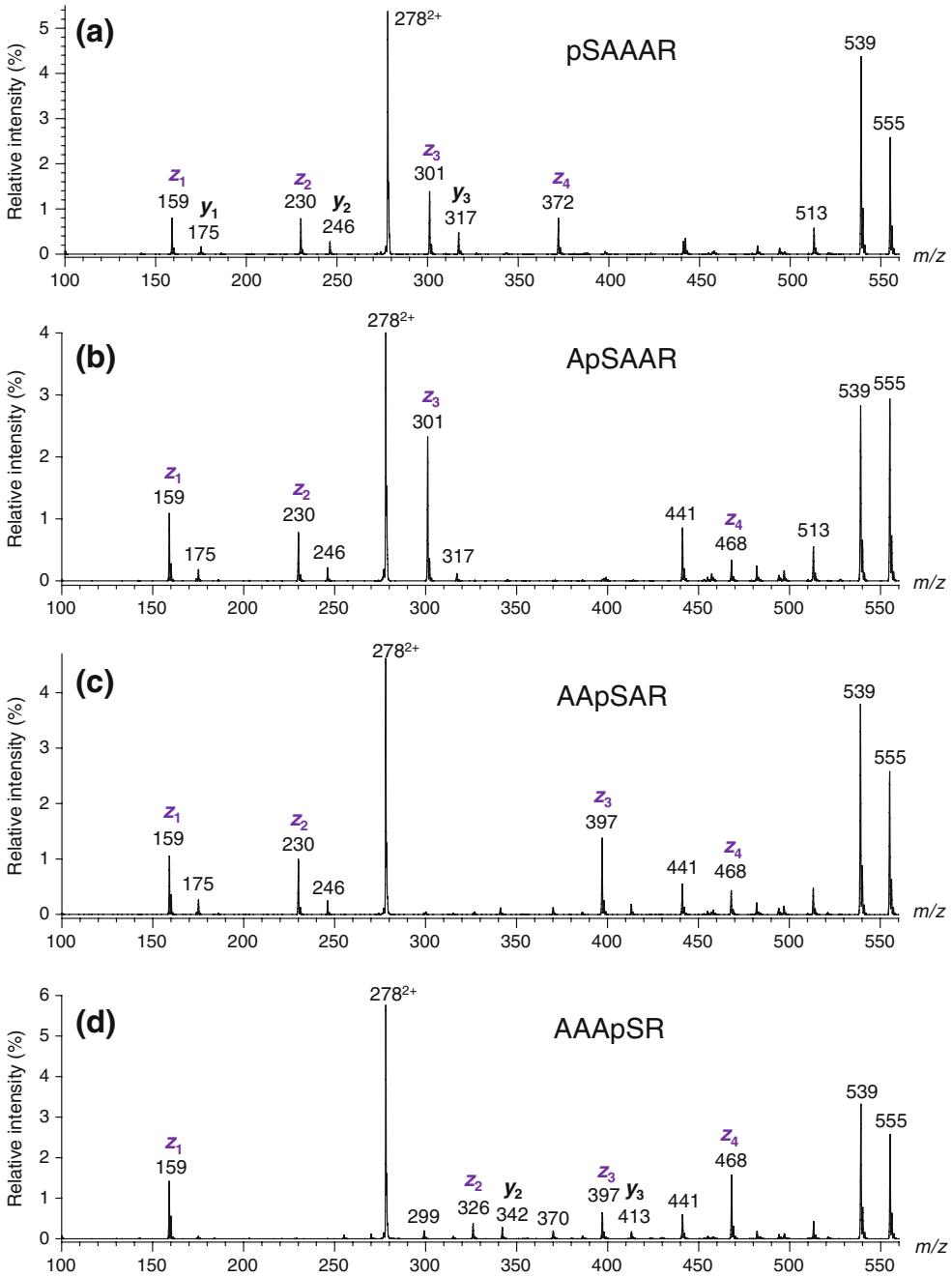

Figure 2. Electron-transfer dissociation mass spectra of **(a)** $(pSAAAR+2H)^{2+}$, **(b)** $(ApSAAR+2H)^{2+}$, **(c)** $(AApSAR+2H)^{2+}$, and **(d)** $(AAApSR+2H)^{2+}$. Electron transfer from fluoranthene anion-radical at 100 ms ion–ion interaction time. The ion relative intensities were normalized to the sum of all charge-reduced ion intensities

ment ions at *m/z* 457, which by mass and elemental composition correspond to loss of an H atom and phosphoric acid from the charge-reduced ions (Figure 3a–d). Weak $(M + H)^+$ ions due to loss of H from the charge-reduced ions appear at *m/z* 555. The ECD spectra display the z_1 through z_3 ions or products of their further dissociation by loss of H_3PO_4 (*m/z* 299 from the z_3 ion from AAApSR) or a H_2PO4 radical (*m/z* 300 from the z_3 ion from AApSAR). However, the dominant fragments are the *m/z* 87.0792 ($C_3H_9N_3$) and 100.0870 ($C_4H_{10}N_3$) ions originating from the arginine side chain. These dissociations will be discussed later in the paper.

Dissociations of z Ions

The relative intensities of z_1–z_5 ions from ETD followed an alternating pattern, depending on the peptide sequence (Figure S1, Supplementary Material). Note that the fragments formed by loss of ammonia are denoted as z_5 ions, because it has been shown previously that loss of ammonia

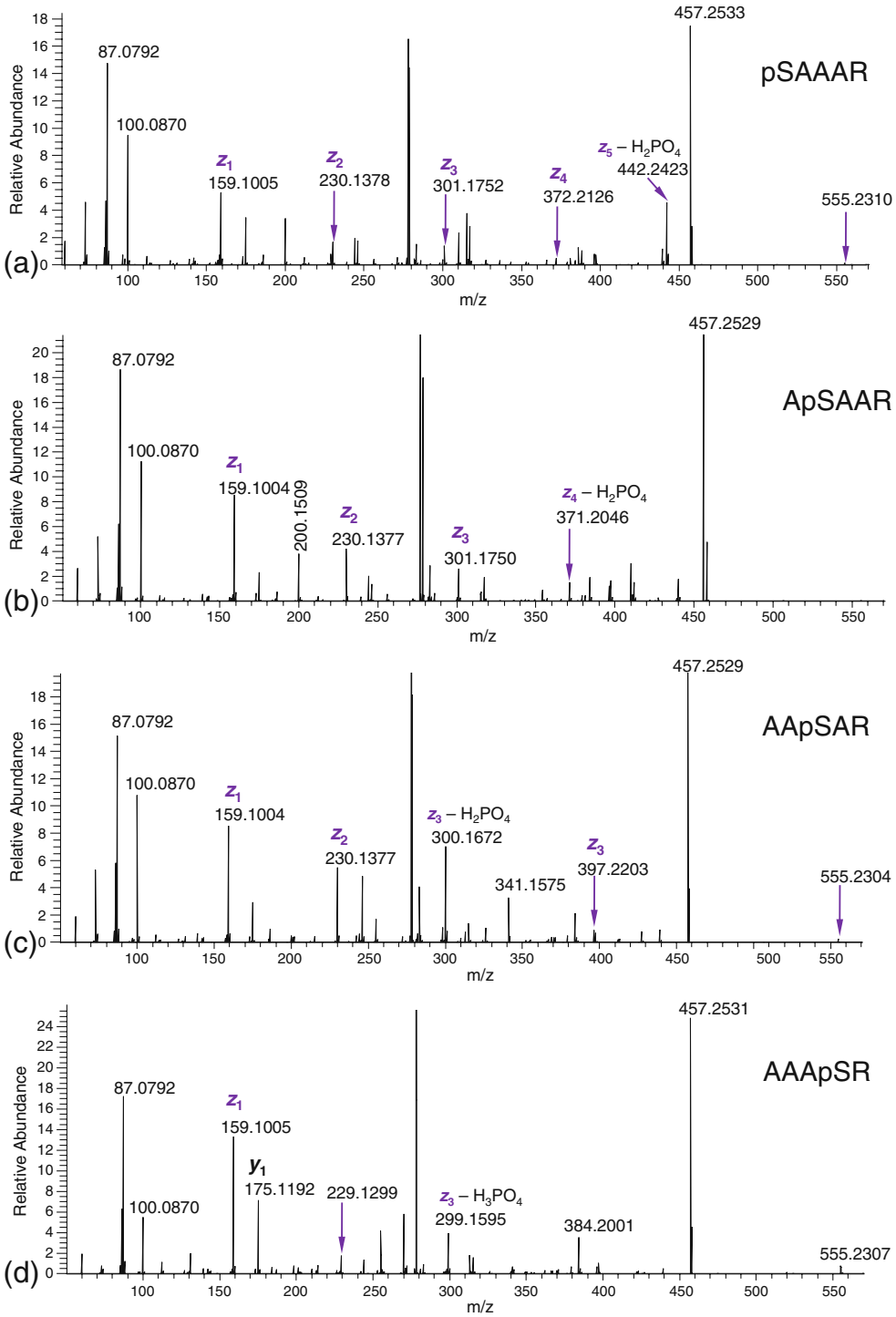

Figure 3. Electron-capture dissociation mass spectra of **(a)** $(pSAAAR+2H)^{2+}$, **(b)** $(ApSAAR+2H)^{2+}$, **(c)** $(AApSAR+2H)^{2+}$, and **(d)** $(AAApSR+2H)^{2+}$ obtained at 300 ms electron-ion interaction time. The ion relative intensities were normalized relative to the precursor ion (*m/z* 278.1182) as 100%

proceeds with high selectivity from peptide N-termini forming C_α radicals which are homologous to regular *z* fragment ions [38]. Of particular interest were dissociations of long-lived *z* ions that were isolated in the ion trap and collisionally activated because they could provide insight into consecutive dissociations following electron attachment [39]. With the present series of phosphopeptides, it is practical to distinguish two types of *z* ions, that is, those that retain the phosphorylated serine residue and those that do not. Their dissociations show interesting features that are represented by the CID-MS^3 spectra of *z* ions from ETD of doubly charged pSAAAR and AAApSR.

Phosphorylated z Ions

The CID-MS^3 spectrum of the z_5 ion from pSAAAR (*m/z* 539) shows an abundant fragment at *m/z* 441 due to an elimination of H_3PO_4 (Figure 4a). The loss of H_3PO_4 competes with cascade backbone dissociations forming the z_4 (*m/z* 372) and z_3 (*m/z* 301) ions, and also with a charge-induced backbone dissociation leading to the y_2 ion at *m/z* 246. The CID-MS^3 spectra of the other terminally phosphorylated *z* ions, e.g., the z_4 ion from ApSAAR (*m/z* 468, Figure 4b), z_3 ion from AApSAR (*m/z* 397, Figure 4c), and z_2 ion from AAApSR (*m/z* 326, Figure 4d) also show losses of H_3PO_4 at *m/z* 370, 299, and 228, respectively, which in these cases are accompanied by loss of a H_2PO_4 radical. Furthermore, these dissociations compete with abundant eliminations of water (e.g., *m/z* 308 from AAApSR z_2), COOH (*m/z* 281), and an arginine side-chain fragmentation giving the $C_4H_{10}N_3$ ion at *m/z* 100. A common feature of these phosphorylated z_5, z_4, z_3, and z_2 ions is that they have the deaminated phosphoserine moiety at the radical terminus of the peptide chain. Contrasting their multi-

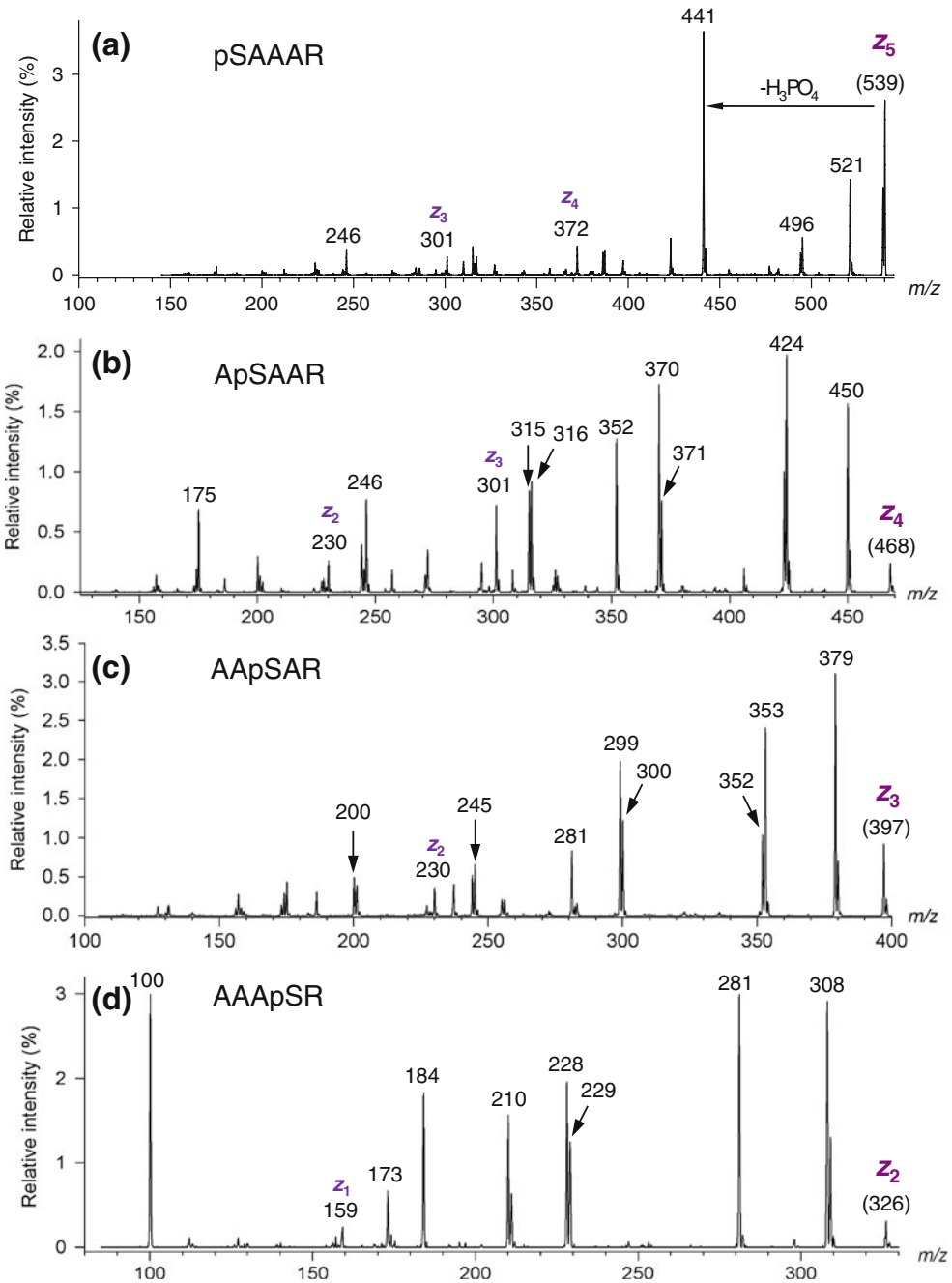

Figure 4. CID-MS^3 mass spectra of **(a)** z_5 ion (*m/z* 539) from ETD of (pSAAAR+2H^{2+}, **(b)** z_4 ion (*m/z* 468) from ETD of (ApSAAR+2H^{2+}, **(c)** z_3 ion (*m/z* 397) from ETD of (AApSAR+2H^{2+}, and **(d)** z_2 ion (*m/z* 326) from ETD of (AAApSR+2H^{2+}. The ion relative intensities were normalized to the sum of fragment ion intensities

channel dissociations, CID-MS^3 of z ions that have internal phosphoserine residues, e.g., the z_3 and z_4 ions from AAApSR, show elimination of H_3PO_4 as the only major dissociation channel (Figure S2, Supplementary Material). This behavior is analogous to CID-MS^3 of even-electron $(M + H)^+$ ions from ETD of the phosphopeptides reported here, which also fragmented by predominant H_3PO_4 elimination (Figure S3, Supplementary Material). Distinct dissociations of z ions are also indicated in the ECD spectra (Figure 3), where the deaminated terminal z ions undergo elimination of H_2PO_4 radicals, as observed for the z_5 ion from pSAAAR, z_4 ion from ApSAAR, z_3 ion from AApSAR, and z_2 ion from AAApSR. In contrast, the z_3 ion from AAApSR, which has an internal phosphoserine moiety, eliminates phosphoric acid.

Non-Phosphorylated z Ions

The CID-MS^3 spectra of the non-phosphorylated z_4 through z_2 ions from pSAAAR also showed interesting backbone fragmentations (Figure 5). For example, the z_4 ion (*m/z* 372) underwent a major elimination of 57, 128, and 199 Da neutral fragments to give the ion series at *m/z* 315, 244, and 173, respectively (Figure 5a). Loss of 57 Da was also observed in the CID spectrum of the z_3 ion where it formed the *m/z* 244 fragment ion (Figure 5b). These backbone fragments formally correspond to $(y_n - 2H)$ ions (n=1–3), and their formation can be visualized by radical-induced reactions involving H-atom migrations analogous to those reported previously for other peptide cation-radicals [40–45]. CID of the z_2 ion results in decarboxylation (*m/z* 186) and Arg side-chain cleavage (*m/z* 100) which both are likely to be radical-driven [41].

Precursor Ion Structures

To shed some light on the properties and dissociations of the charge-reduced phosphopeptide ions, we obtained optimized structures of both precursor dications and charge-reduced ions. To locate global energy minima for precursor dications, we performed an exhaustive search of the conformational space for each peptide sequence. The presence of the C-terminal arginine residue in all these peptides mandates protonation in the basic guanidine group. The other proton

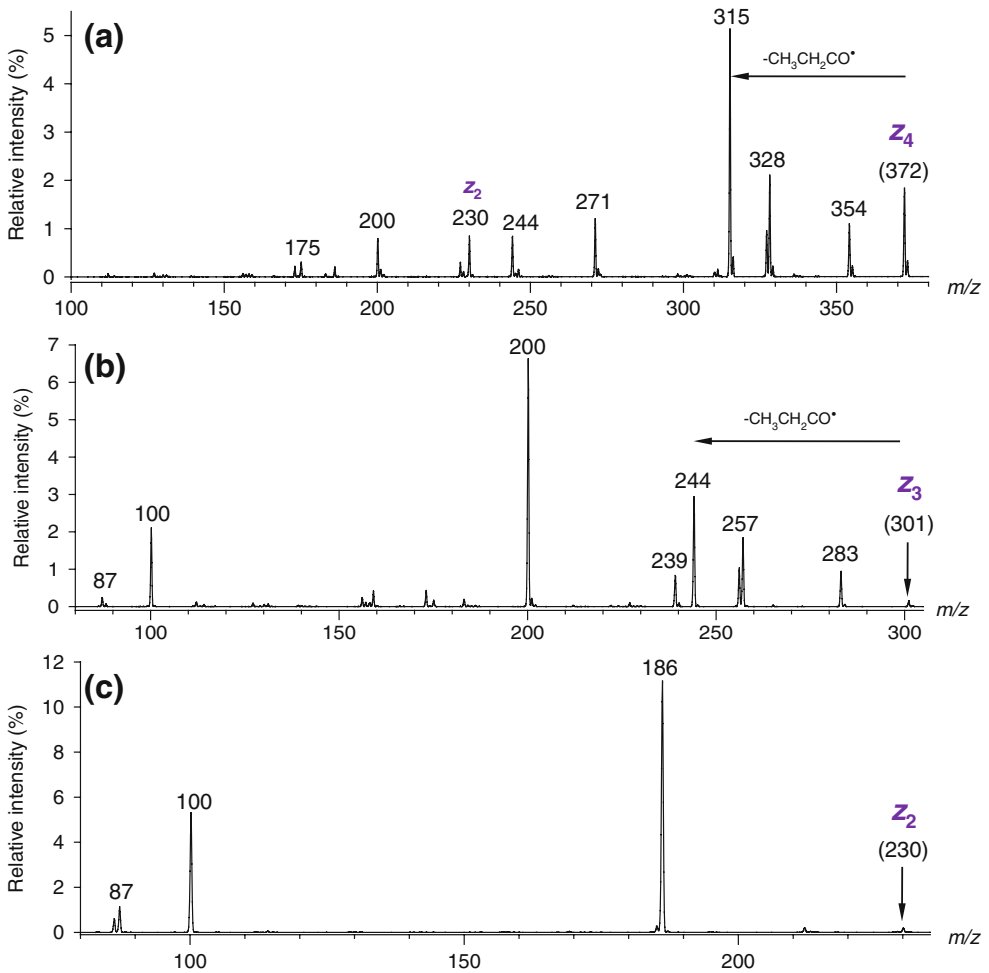

Figure 5. CID-MS^3 mass spectra **(a)** z_4 (*m/z* 539), **(b)** z_3 (*m/z* 301), and **(c)** z_2 (*m/z* 230) ions from ETD of (pSAAAR+2H^{2+}. The ion relative intensities were normalized to the sum of fragment ion intensities

was placed on the N-terminal amino group. The conformers were ranked by their free energies according to combined B3LYP and MP2/6-311++G(2d,p) single-point calculations. The relative enthalpies and free energies of five most stable dication conformers for each sequence are summarized in Table 1. Selected optimized structures are shown in Figure 6, and the remaining structures listed in Table 1 are given as Supplementary Material. The $(pSAAAR + 2H)^{2+}$ ions gave structure $\mathbf{1a}^{2+}$ as the global energy minimum according to both B3LYP and MP2 calculations. A second conformer ($\mathbf{1b}^{2+}$) was calculated to be 7.6 kJ mol^{-1} less stable than $\mathbf{1a}^{2+}$.

However, because of less tight folding $\mathbf{1b}^{2+}$ had a higher entropy than $\mathbf{1a}^{2+}$ so that both conformers were nearly isoenergetic on the free energy scale. The other structures that we investigated (e.g., $\mathbf{1c}^{2+}$–$\mathbf{1e}^{2+}$) were less stable. The fully optimized structures of $\mathbf{1a}^{2+}$ and $\mathbf{1b}^{2+}$ are shown in Figure 6. The phosphate group in both $\mathbf{1a}^{2+}$ and $\mathbf{1b}^{2+}$ is engaged in strong hydrogen bonding, although the patterns differ. In $\mathbf{1a}^{2+}$, the phosphate group is chelated by two hydrogen bonds to the C-terminal carboxyl, while in $\mathbf{1b}^{2+}$ the phosphate internally solvates the N-terminal ammonium group. Overall, $\mathbf{1a}^{2+}$ and $\mathbf{1b}^{2+}$ can be characterized as globular conformers. Of the low-energy conformers of $(ApSAAR+2H)^{2+}$ ions, structures $\mathbf{2a}^{2+}$ and $\mathbf{2b}^{2+}$ had lowest enthalpies and free energies. Both these conformers have strong hydrogen bonds between the phosphate and N-terminal ammonium groups. A similar arrangement was found for the two lowest-energy conformers of $(AApSAR+2H)^{2+}$ ($\mathbf{3a}^{2+}$ and $\mathbf{3b}^{2+}$, Figure 6). Interestingly, the low-energy conformers of ions $\mathbf{2}^{2+}$ and $\mathbf{3}^{2+}$ have structures with extended peptide backbones. Finally, $(AAApSR+2H)^{2+}$ ions were calculated to assume three low-energy conformations ($\mathbf{4a}^{2+}$–$\mathbf{4c}^{2+}$, Figure 6) in which the phosphate group internally solvated the N-terminal ammonium, but which differed in the H-bonding networks of the neutral amide groups. Conformers $\mathbf{4a}^{2+}$–$\mathbf{4c}^{2+}$ can be characterized as globular structures.

Regarding the relative energies of the sequence isomers, ion $\mathbf{3a}^{2+}$ was found to be the global energy minimum followed by $\mathbf{2a}^{2+}$ (+7 kJ mol^{-1}), $\mathbf{4a}^{2+}$ (+18 kJ mol^{-1}), and $\mathbf{1a}^{2+}$ (+29 kJ mol^{-1}). This order of relative stabilities reflects the Coulomb repulsion of the charged groups as well as the attractive dipolar and H-bonding interactions of the charged and neutral groups in the peptide dications, which are restrained by the position of the phosphoserine residue in the sequence. The magnitude of the Coulomb repulsion can be gauged by the calculated distances between the ammonium nitrogen and guanidinium central carbon atoms in the most stable conformers, which were 6.9, 16.7, 14.4, and 11.1 Å in $\mathbf{1a}^{2+}$, $\mathbf{2a}^{2+}$, $\mathbf{3a}^{2+}$, and $\mathbf{4a}^{2+}$, respectively. Thus, it appears that Coulomb repulsion is the dominant energy term destabilizing the pSAAAR ions.

Another interesting feature of the ion structures is that none of the low-energy conformers displayed a H-bonding interaction between the neutral phosphate and charged guanidinium group. Such interactions have been considered to explain the stability of arginine-phosphopeptide ion clusters [46–48] but do not seem to play a role in isolated peptide ions in which the phosphate group is neutral. This is presumably due to the donor-acceptor nature of the neutral phosphate group, where the P = O oxygen atom serves as a p-electron donor in solvating acidic protons of the peptide groups, and the acidic P-OH protons are internally solvated by suitable electron donors from the peptide amide or carboxyl groups. This appears to be more favorably realized by phosphate H-bonding to the ammonium group in low-energy conformers of $\mathbf{1}^{2+}$–$\mathbf{4}^{2+}$ than by H-bonding to the guanidinium ion. Coulomb attraction may be another stabilizing factor, because the NH_3 and H_2PO_4 groups carry substantial partial positive and negative charge, e.g., +0.64 and –0.32, respectively, in $\mathbf{2a}^{2+}$.

A feature related to the charge distribution in the dications studied here is that they all have substantial dipole moments. For example, $\mathbf{1a}^{2+}$ was calculated to have a dipole moment of 11.1 D, which was roughly aligned along the axis connecting the phosphate P and guanidinium C atoms, with the negative end at the phosphate group. Likewise, ions $\mathbf{2a}^{2+}$, $\mathbf{3a}^{2+}$, and $\mathbf{4a}^{2+}$ had dipole moments of 10.4, 9.3, and 11.5 D, which were aligned along the axis connecting the phosphate P and guanidinium C atoms, with the negative end at the phosphate group. This feature may be important in affecting electron attachment in ECD [23], as discussed later.

Table 1. Relative energies of phosphopeptide dications

Ion	Relative energy[a,b]			
	B3LYP	B3LYP	MP2	B3-MP2
	6-31+G(d,p)	6-311++G(2d,p)		
$\mathbf{1a}^{2+}$	0.0	0.0	0.0	0.0 (0)[c] (0)[d]
$\mathbf{1b}^{2+}$	7.2	9.4	5.8	7.6 (7.5)[c] (0.8)[d]
$\mathbf{1c}^{2+}$	8.5	10	9.8	10 (10)[c] (4.6)[d]
$\mathbf{1d}^{2+}$	11	13	11	12 (12)[c] (7.7)[d]
$\mathbf{1e}^{2+}$	14	15	21	18 (18)[c] (8.7)[d]
$\mathbf{2a}^{2+}$	0.0	0.0	0.0	0.0 (0)[c] (0)[d]
$\mathbf{2b}^{2+}$	3.6	3.6	4.5	4.1 (4.3)[c] (2.9)[d]
$\mathbf{2c}^{2+}$	8.5	9.6	1.1	5.3 (5.6)[c] (6.1)[d]
$\mathbf{2d}^{2+}$	10	10	12	11 (12)[c] (7.6)[d]
$\mathbf{2e}^{2+}$	9.7	8,2	16	12
$\mathbf{3a}^{2+}$	0.0	0.0	0.0	0.0 (0)[c] (0)[d]
$\mathbf{3b}^{2+}$	6.7	6.3	5.6	6.0 (5.4)[c] (9.7)[d]
$\mathbf{3c}^{2+}$	10	9.8	13	11 (12)[c] (10)[d]
$\mathbf{3d}^{2+}$	15	15	24	20 (21)[c] (21)[d]
$\mathbf{3e}^{2+}$	21	24	4.5	14 (15)[c] (33)[d]
$\mathbf{4a}^{2+}$	3.2	0.9	–1.1	–0.1 (1.3)[c] (–3.1)[d]
$\mathbf{4b}^{2+}$	0.0	0.0	0.0	0.0 (0)[c] (0)[d]
$\mathbf{4c}^{2+}$	2.4	1.0	–16	–7.4 (–8.8)[c] (0.7)[d]
$\mathbf{4d}^{2+}$	15	12	22	17 (18)[c] (13)[d]
$\mathbf{4e}^{2+}$	22	22	–1.5	11 (11)[c] (19)[d]

[a]In units of kJ mol^{-1}.
[b]Including B3LYP/6-31+G(d,p) zero point energies and referring to 0 K unless stated otherwise. [c] Relative enthalpies at 298 K.
[d]Relative free energies at 298 K.

Charge-Reduced Ions

The optimized precursor ion structures served as starting points for geometry optimization of cation-radical structures

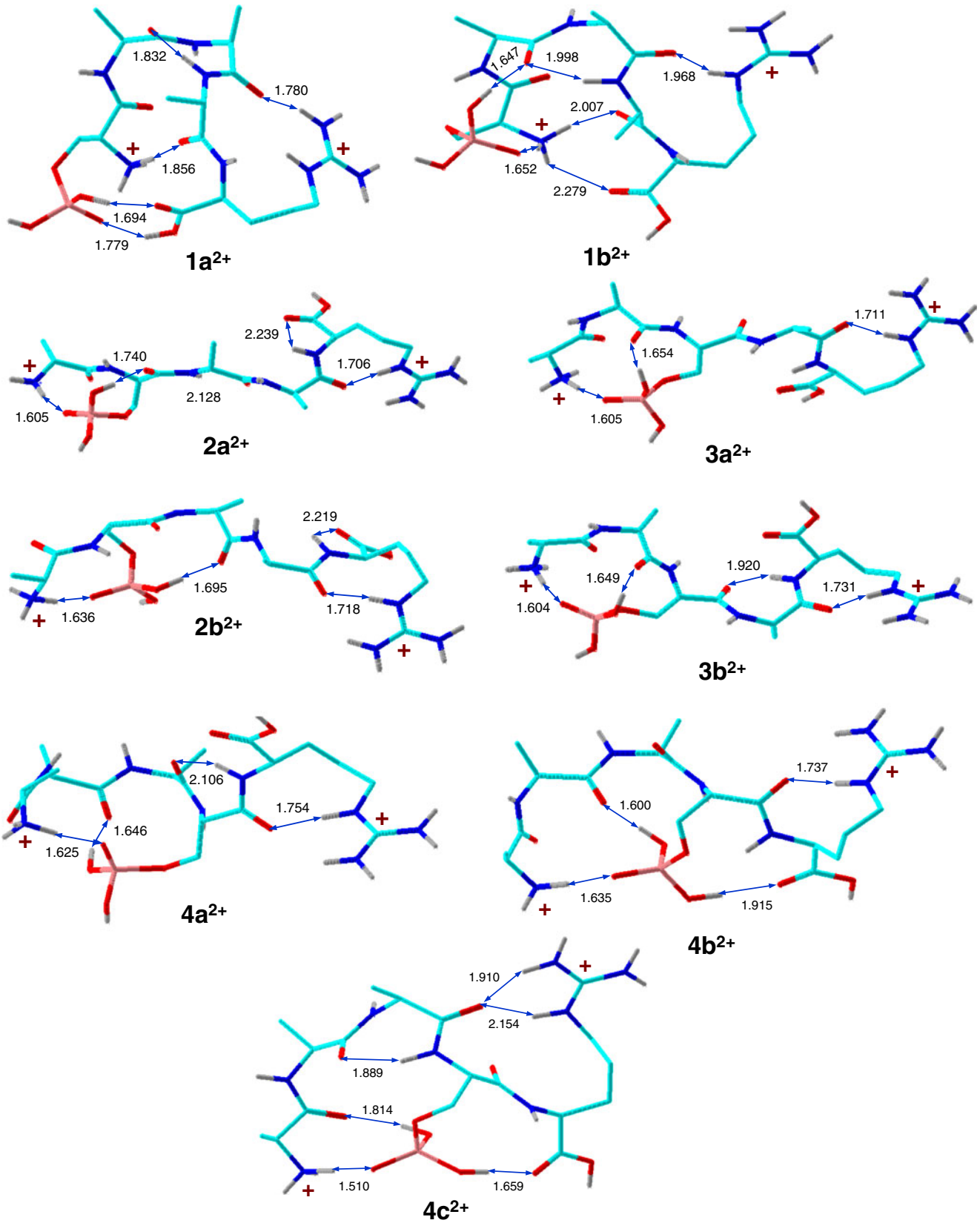

Figure 6. B3LYP/6-31+G(d,p) optimized structures of lowest-energy conformers for $(pSAAAR+2H)^{2+}$, $(ApSAAR+2H)^{2+}$, $(AApSAR+2H)^{2+}$, and $(AAApSR+2H)^{2+}$. The atoms are color-coded as follows: turquoise = C, blue = N, red = O, gray = H. Aliphatic hydrogen atoms are not shown. Hydrogen bonds are denoted by double-headed blue arrows, the distances are in Ångstrøms

for the charge reduced ions. Electron attachment to $\mathbf{1a}^{2+}$ followed by geometry optimization resulted in a spontaneous migration of an ammonium proton to the Ala_4 amide oxygen forming aminoketyl radical $\mathbf{1a}^{+\bullet}$ (Scheme 1). The electron attachment to $\mathbf{1a}^{2+}$ is expected to exhibit large Franck-Condon effects as judged from the difference between the vertical recombination energy, RE_v=4.81 eV and the adiabatic value, RE_a=5.99 eV. However, the adiabatic value includes the bond reorganization due to the exothermic proton migration from the ammonium to the amide carbonyl. Structure $\mathbf{1a}^{+\bullet}$ is indicative of a dissociation of the N–C_α bond between the Ala_4 and Arg residues leading to the z_1 fragment ion which is observed in ETD, ECID, and ECD mass spectra. The electronic structure of the vertically formed ion, denoted as $(\mathbf{1a}^{+\bullet})$*, is shown in Figure S4. Note that $(\mathbf{1a}^{+\bullet})$* is not a local energy minimum but a transient high-energy point on the potential energy surface of the charge-reduced which is accessed by vertical electron transfer. The odd-electron density distribution in the lowest electronic state of $(\mathbf{1a}^{+\bullet})$* points to spin accumulation in the guanidinium group (26%), carboxyl (18%), serine amide (14%), and Ala_4 amide (13%). The N-terminal ammonium (9%), Ala_2 amide (5%), Ala_3 amide (4%), and the phosphate group (2%) account for a minor part of spin density. The substantial odd-electron density in the Ala_4 amide group is indicative of the spontaneous proton transfer upon geometry relaxation to $\mathbf{1a}^{+\bullet}$.

Electron attachment to the other conformer $\mathbf{1b}^{2+}$ also resulted in spontaneous isomerization upon geometry optimization. This involved a proton transfer from the N-terminal ammonium to the Ala_2 amide which was coupled with a phosphate proton moving to the ammonium group. The resulting local energy minimum $(\mathbf{1b}^{+\bullet})$ is a zwitterionic cation-radical which has the spin density localized within the

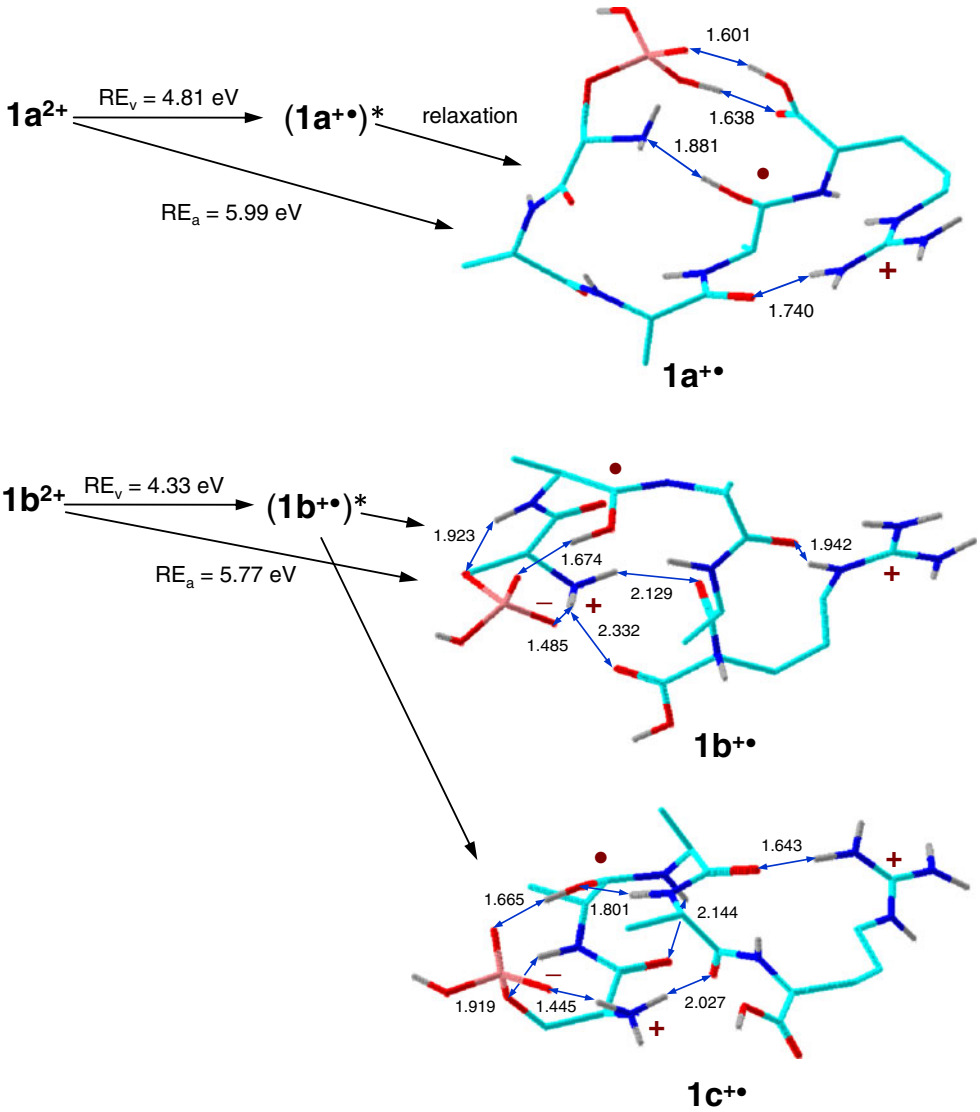

Scheme **1.** Energetics of electron attachment to $(pSAAAR+2H)^{2+}$ and B3LYP/6-31+G(d,p) optimized structures of charge-reduced ions $\mathbf{1a}^{+\bullet}$–$\mathbf{1c}^{+\bullet}$

Ala_2 aminoketyl radical moiety. The N-terminal ammonium cation and the phosphate anion form a tight ion pair, which is bound by a short H-bond at 1.485 Å (Scheme 1). Another zwitterion was found as a local energy minimum ($\mathbf{1c}^{+\bullet}$) which was nearly isoenergetic with $\mathbf{1b}^{+\bullet}$ but had a different H-bonding pattern for one of the ammonium protons (Scheme 1).

Electron transfer to ions $\mathbf{2a}^{2+}$ and $\mathbf{2b}^{2+}$ followed by geometry relaxation furnished two different cation-radicals (Scheme 2). The cation-radical from $\mathbf{2a}^{2+}$ was a zwitterion ($\mathbf{2a}^{+\bullet}$), which showed a positively charged N-terminal ammonium group which was hydrogen bonded to the neutral phosphate and the Ala_1 amide anion-radical. The other charging proton was sequestered by the arginine guanidinium group which was not reduced. Structure $\mathbf{2a}^{+\bullet}$ represents another example of a local energy minimum corresponding to a charge-stabilized amide π* state as suggested previously [49–51]. The other cation-radical ($\mathbf{2b}^{+\bullet}$) was a standard guanidinium radical [52] resulting from one-electron reduction in the arginine residue. Classic structure $\mathbf{2b}^{+\bullet}$ was 20 kJ mol^{-1} more stable than zwitterion $\mathbf{2a}^{+\bullet}$.

Two different structures developed upon geometry optimization of charge-reduced $\mathbf{3a}^{2+}$ and $\mathbf{3b}^{2+}$ (Scheme 3) The first one ($\mathbf{3a}^{+\bullet}$), which was produced from $\mathbf{3a}^{2+}$, was an aminoketyl radical that was formed by a relay migration of a phosphate proton onto the Ala_2 amide carbonyl accompanied by a shift of one ammonium proton to recreate a neutral phosphate group. The other cation-radical ($\mathbf{3b}^{+\bullet}$) was a conformer whose formation from $\mathbf{3b}^{2+}$ can be viewed analogously to that of $\mathbf{3a}^{+\bullet}$. Charge-reduced zwitterions that maintain the N-terminal ammonium group are prone to a highly exothermic loss of NH_3, which can proceed through ion-molecule complexes, such as $\mathbf{3c}^{+\bullet}$ [53].

The cation-radicals formed upon electron attachment to ions $\mathbf{4a}^{2+}$–$\mathbf{4c}^{2+}$ were all zwitterions that contained an N-terminal ammonium tightly H-bonded to the phosphate anion group (Scheme 4). The formation of structures $\mathbf{4a}^{+\bullet}$–$\mathbf{4c}^{+\bullet}$ can be viewed as a simple migration of a phosphate proton onto the carbonyl anion-radical intermediate produced by electron attachment. The proton receptor groups were the Ala_2 amide, the carboxyl group, and the Ala_1 amide in $\mathbf{4a}^{+\bullet}$, $\mathbf{4b}^{+\bullet}$, and $\mathbf{4c}^{+\bullet}$, respectively. The proton migration upon the formation of $\mathbf{4a}^{+\bullet}$ and $\mathbf{4b}^{+\bullet}$ correlates with the phosphate group H-bonding pattern in the precursor ions. In $\mathbf{4c}^{+\bullet}$, the migration presumably follows a different route and may involve a tandem shift of the N-terminal ammonium and phosphate protons. These pathways occur spontaneously and to distinguish them would require performing reaction dynamics calculations which are beyond our computational resources for systems of this size.

Mechanisms for z-Ion Dissociations

The above-presented spectra showed that ECD of the phosphopeptide ions and CID-MS^3 of the phosphate-containing *z* ions induced different types of phosphoric acid elimination, depending on whether it proceeded from an internal or deaminated terminal phosphoserine residue, possibly indicating different mechanisms for these dissociations. One of the previously suggested mechanisms of H_3PO_4 elimination from serine containing phosphopeptide ions assumed a charge-remote β-elimination involving transfer of an H_α atom and formation of a dehydroalanine residue [54, 55]. This mechanism has been shown to be inconsistent with newer labeling data and CID-MS^3 investigation of product ions. A more likely mechanism involves proton-induced elimination with neighboring participation of amino [56] or amide groups [57] from the N-terminal site of the phosphoserine residue, as recently reviewed [58]. Obviously, none of these mechanisms can apply to the elimination of phosphoric acid from deaminated serine residues in the *z* ions, which have vinylic α-hydrogen atoms and are missing the N-terminal functional groups. The concurrent elimination of a $H_2PO_4^{\bullet}$ radical, which is not observed for the *z* ions with internal phosphoserine residues, suggests a radical mechanism. One possibility is that the C_α radical center at the deaminated serine residue weakens the CH_2–OPO_3H_2 bond that dissociates upon collisional activation. The $H_2PO_4^{\bullet}$ radical then may either depart or abstract a

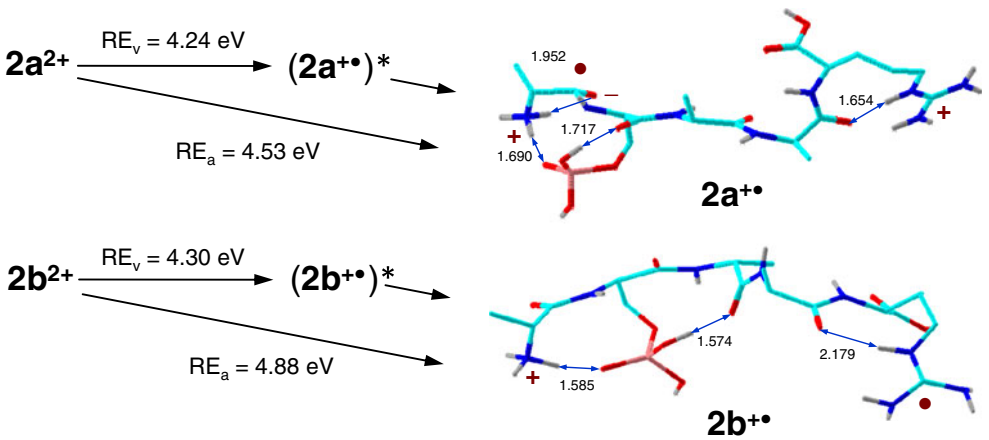

Scheme **2.** Energetics of electron attachment to $(ApSAAR+2H)^{2+}$ and B3LYP/6-31+G(d,p) optimized structures of charge-reduced ions $\mathbf{2a}^{+\bullet}$ and $\mathbf{2b}^{+\bullet}$

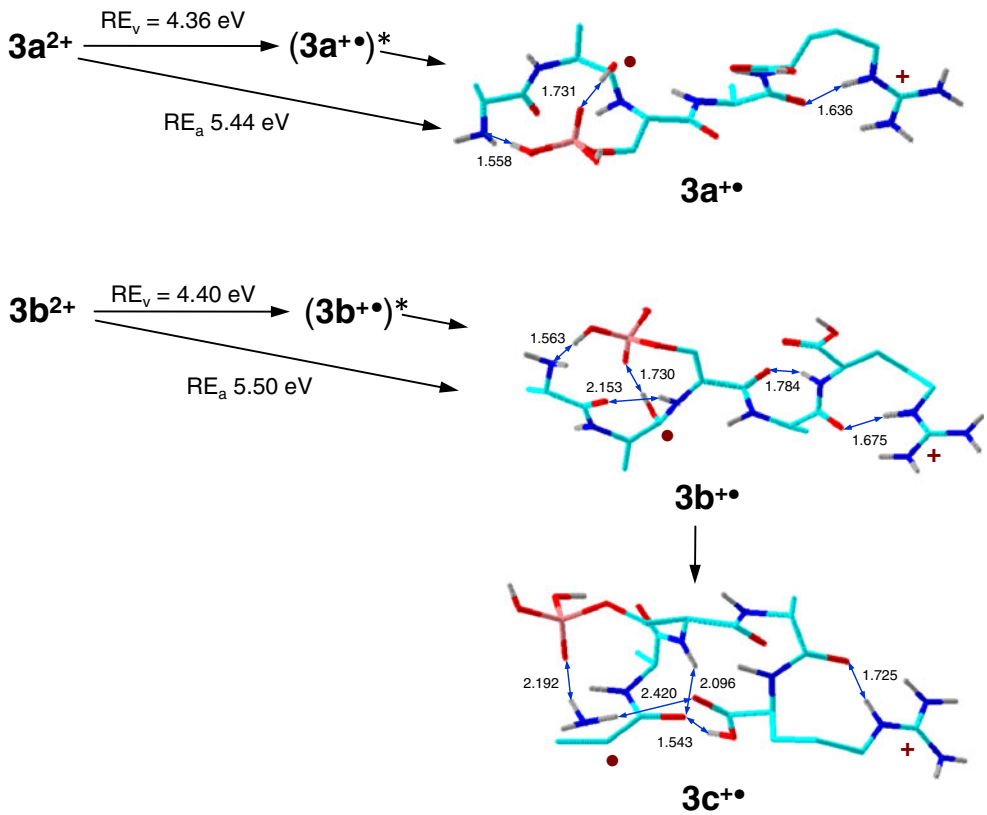

Scheme **3.** Energetics of electron attachment to $(AApSAR+2H)^{2+}$ and B3LYP/6-31+G(d,p) optimized structures of charge-reduced ions **3a**$^{+\bullet}$–**3c**$^{+\bullet}$

hydrogen atom from the peptide residue. We calculated the H-atom affinity of $H_2PO_4^{\bullet}$ as $\Delta H_{aff,0}$=457 kJ mol^{-1} (from combined B3LYP and MP2/6-311++G(2d,p) single point energies), which indicated that $H_2PO_4^{\bullet}$ can exothermically abstract not only the relatively weakly bound peptide H_α atoms ($\Delta H_{aff,0}$=345–400 kJ mol^{-1})[59, 60], but also those from aliphatic side chains ($\Delta H_{aff,0}$ <440 kJ mol^{-1}) [61]. An alternative mechanism would assume a cyclic transition state where the cleavage of the CH_2–OPO_3H_2 bond is accompanied by one of the phosphate O atoms abstracting an H atom from a sterically accessible site.

We investigated these mechanisms by electron structure theory calculations on the smaller z_2 ion (**5a**) from AAApSR which shows eliminations of both H_3PO_4 and $H_2PO_4^{\bullet}$ (Scheme 5). A late transition state (**TS1**) was found for the cleavage of the CH_2–OPO_3H_2 bond at a C–O distance of 2.928 Å, which was 117 kJ mol^{-1} above **5a** (Table 2). The H_2PO_4 radical remained hydrogen-bonded to the arginine side chain of the peptide fragment ion, forming an ion-radical complex (**5b**), which was 106 kJ mol^{-1} above **5a**. The threshold energy for the loss of H_2PO_4 from **5a** was calculated as ΔH_0=139 kJ mo^{-1} to give fragment **5c**, representing the *m/z* 229 ion. The noncovalent binding of the H_2PO_4 radical to the peptide fragment ion presumably facilitates a hydrogen atom transfer required for the loss of phosphoric acid to form the *m/z* 228 ion. Although we did not study all possible mechanisms for such an H-atom migration, we note that abstraction of the arginine H_α atom by the H_2PO_4 radical was 115 kJ mol^{-1} exothermic and thus energetically favored, forming phosphoric acid and the peptide fragment ion **5e**. The fact that both the loss of H_2PO_4 and elimination of H_3PO_4 were observed experimentally indicated that these occurred as competitive dissociations of complex **5b**. The reaction path to the arginine H_α atom abstraction by the H-bonded H_2PO_4 radical can proceed through **TS2**, which was 32 kJ mol^{-1} above **5b** (138 kJ mol^{-1} relative to **5a**, Table 2). The hydrogen transfer first forms a very stable non-covalent complex of phosphoric acid with the incipient peptide fragment (**5d**), which requires 93 kJ mol^{-1} to eliminate phosphoric acid to form **5e** (Scheme 5).

Regarding non-phosphorylated *z* ions, we did not study all their radical-induced fragmentations in detail here. Previous work indicated that H-atom transfers in *z* ions were facile and required small energy barriers including those for backbone amide *cis-trans* isomerizations [41]. For example, a transfer of the H_α atom from Ala_3 to the terminal C_α position in the z_4 ion from pSAAAR (Structure **6a**) requires a prior trans-to-cis isomerization of the Ala_2 amide group to form ion **6b** (Scheme 6). This ion isomer undergoes a H_α atom transfer which requires 65 kJ mol^{-1} in **TS3** (101 kJ mol^{-1} relative to **6a**), forming the isomeric Ala_3 C_α radical (**6c**) with a terminal CH_3CH_2CO group. Note that **6c** is nearly isoenergetic with the trans-z_4 ion **6a** (Table 3).

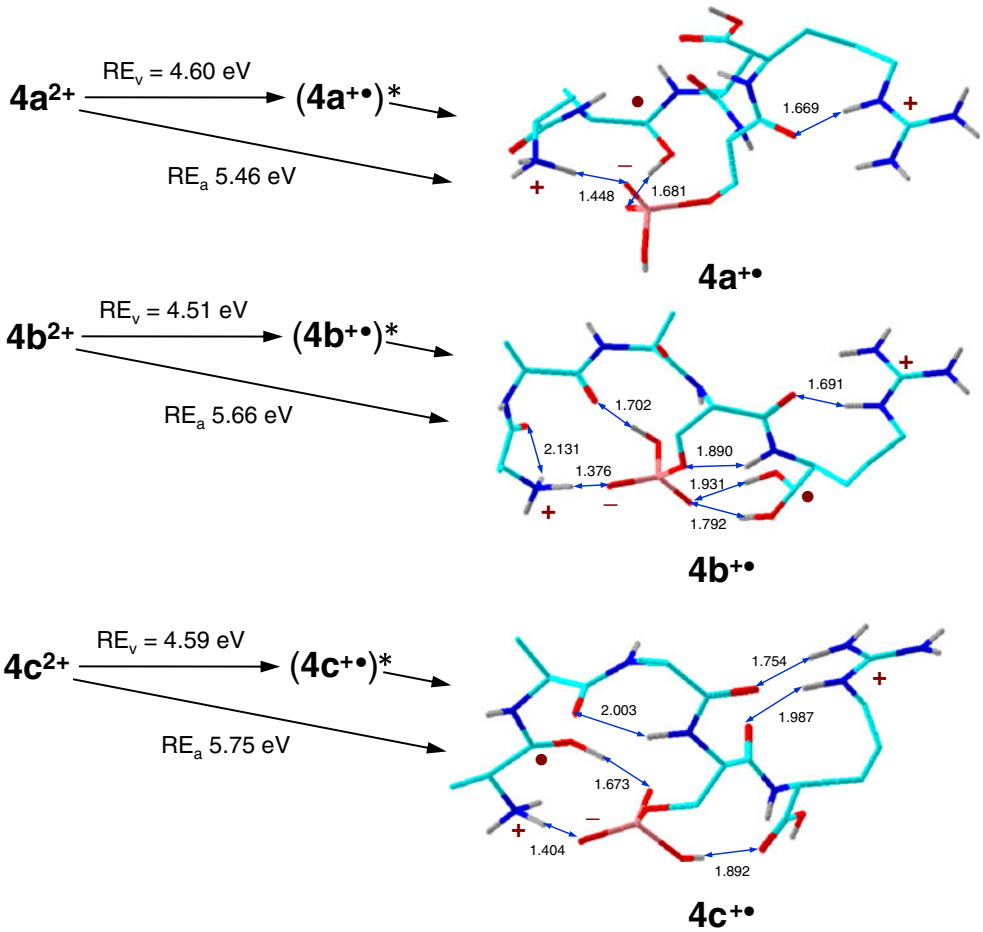

Scheme **4.** Energetics of electron attachment to $(AAApSR+2H)^{2+}$ and B3LYP/6-31+G(d,p) optimized structures of charge-reduced ions **4a$^{+\bullet}$–4c$^{+\bullet}$**

Cleavage of the CH_3CH_2CO–N bond in ion **6c** proceeds through **TS4**, which is 126 kJ mo^{-1} above **6a**, to eliminate a propionyl radical and forming the *m/z* 315 fragment ion (**6d**). An alternative pathway may involve amide *cis* → *trans* isomerization in **6c** followed by CO–N bond cleavage through **TS5** (E_{TS5}=100 kJ mol^{-1}) yielding fragment ion **6e**, which is energetically more favorable than dissociation through **TS4** (Table 3).

The calculated TS energies show that the C_α radical sites generated by H-atom migrations in ***z*** ions (e.g., **6c**) weaken the adjacent amide C–N bond to promote elimination of acyl radicals such as $CH_3CH_2CO^\bullet$. A similar effect presumably promotes the loss of $CH_3CH_2CONHCH(CH_3)CO^\bullet$ (**6f**) forming the *m/z* 244 fragment ion (**6 g**). The TS energies (Table 3) further indicate that the rate determining step is the H-atom migration. We note that an analogous scheme has been proposed by McLuckey and coworkers for the dissociation of a z_4 ion from a VDFVNFK heptapeptide [39]. However, their z_4(VNFK) ion underwent a preferential loss of a $CONH_2$ radical by a C_β–C_γ side-chain bond cleavage in the Asn residue, which >10-fold outcompeted the peptide C–N bond dissociation [39]. Hence, side-chain groups can be expected to have a major effect on the radical-induced backbone dissociations of peptide ***z*** ions. Evidently, the Ala methyl groups in our peptide radicals are not prone to losses of H atoms by β-fission and, therefore, backbone cleavages are favored.

Discussion

Electron capture and transfer caused conspicuously different dissociations of the phosphorylated pentapeptide ions. To recapitulate the major dissociations, electron capture resulted in loss of an H atom followed by elimination of phosphoric acid. Radical-induced dissociations upon electron capture mainly occurred in the arginine side chain and in the peptide backbone. Contrasting these, electron transfer from both Cs atoms and fluoranthene anion-radicals induced mainly backbone N–C_α bond dissociations forming ***z*** ion series. Loss of H and ammonia also occurred, whereas elimination of phosphoric acid was minor. Some of these effects can be explained by the different energetics and time scales of the three sets of experiments reported here. For example, the time scale for charge-reduced ion dissociations in ECID is ca. 5 μs as opposed to 100–200 ms in ETD. This can account for the observation of non-dissociating charge-

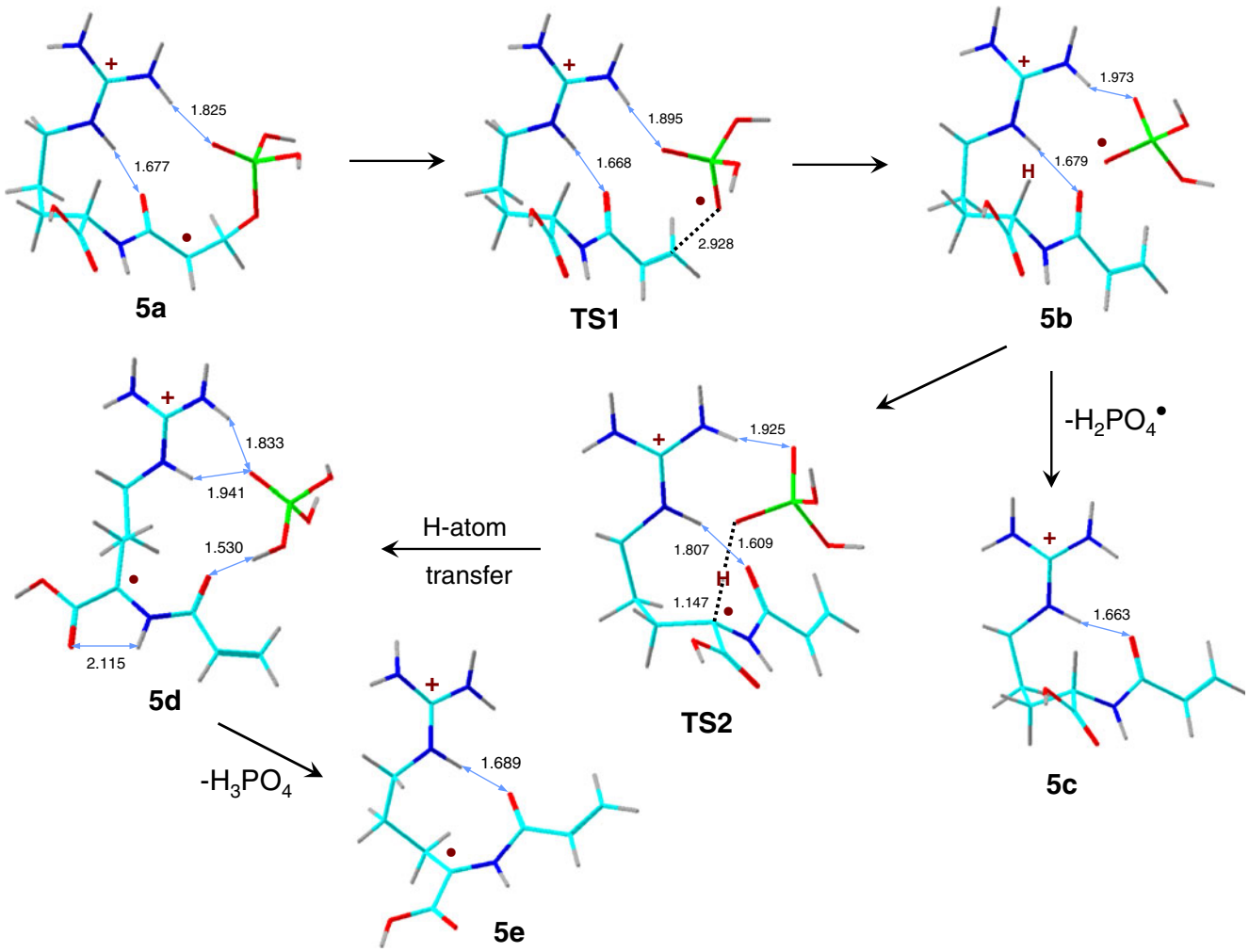

Scheme **5.** Dissociations of z_2 ions from AAApSR

reduced ions in ECID but not in ETD. Another quantitative difference between the ECID and ETD data is the substantially larger relative abundance of loss of ammonia in the former type of spectra. This can be related to the different energetics of electron transfer from Cs and fluoranthene anion-radicals.

Electron Attachment Energetics

Collisional electron transfer from a Cs atom can be described by an energy balance equation (ΔE, Equation 1), which contains the ion vertical recombination energy, RE_v(ion), the Cs ionization energy, IE(Cs)=3.894 eV, a Coulomb term for the repulsive potential of the charge-reduced peptide ion and Cs cation in the product channel, and the attractive ion-induced dipole potential in the reactant channel at critical distance R_c where electron transfer takes place [62]. Positive ΔE means that the electron transfer is exothermic.

$$\Delta E = RE_v(ion) - IE(Cs) - \left[\frac{(ze)^2}{4\pi\varepsilon_0 R_c} + \frac{\alpha(z+1)^2 e^2}{32\pi^2\varepsilon_0^2 R_c^4}\right] \quad (1)$$

Based on the pentapeptide ion diameter (ca. 20 Å) and the Cs atom radius (3.34 Å), electron transfer must occur at $R_c \geq$ 25 Å, where the ion-induced dipole potential becomes small (0.0044 eV) and can be neglected, despite the large Cs atom polarizability ($\alpha = 6.61 \times 10^{-39}$ C m V^{-1}). The energy balance

Table 2. Relative and dissociation energies of phosphorylated z_2 fragment ions from AAApSR

	Relative energy[a,b]			
	B3LYP	B3LYP	PMP2	B3-PMP2[c]
Ion or Reaction	6-31+G(d,p)	6-311++G(2d,p)		
5a	0	0	0	0
5b	79	72	140	106
TS1	93	87	146	117
TS2	99	95	181	138
5d	–79	–86	–51	–68
5c+$H_2PO_4^•$	122	109	170	139
5e+H_3PO_4	15	0.4	49	25

[a]In units of kJ mol^{-1}.
[b]Including B3LYP/6-31+G(d,p) zero-point energy corrections and referring to 0 K.
[c]E[B3-PMP2]=0.5{E[B3LYP/6-311++G(2d,p)] + E[PMP2/6-311++G(2d,p)]}.

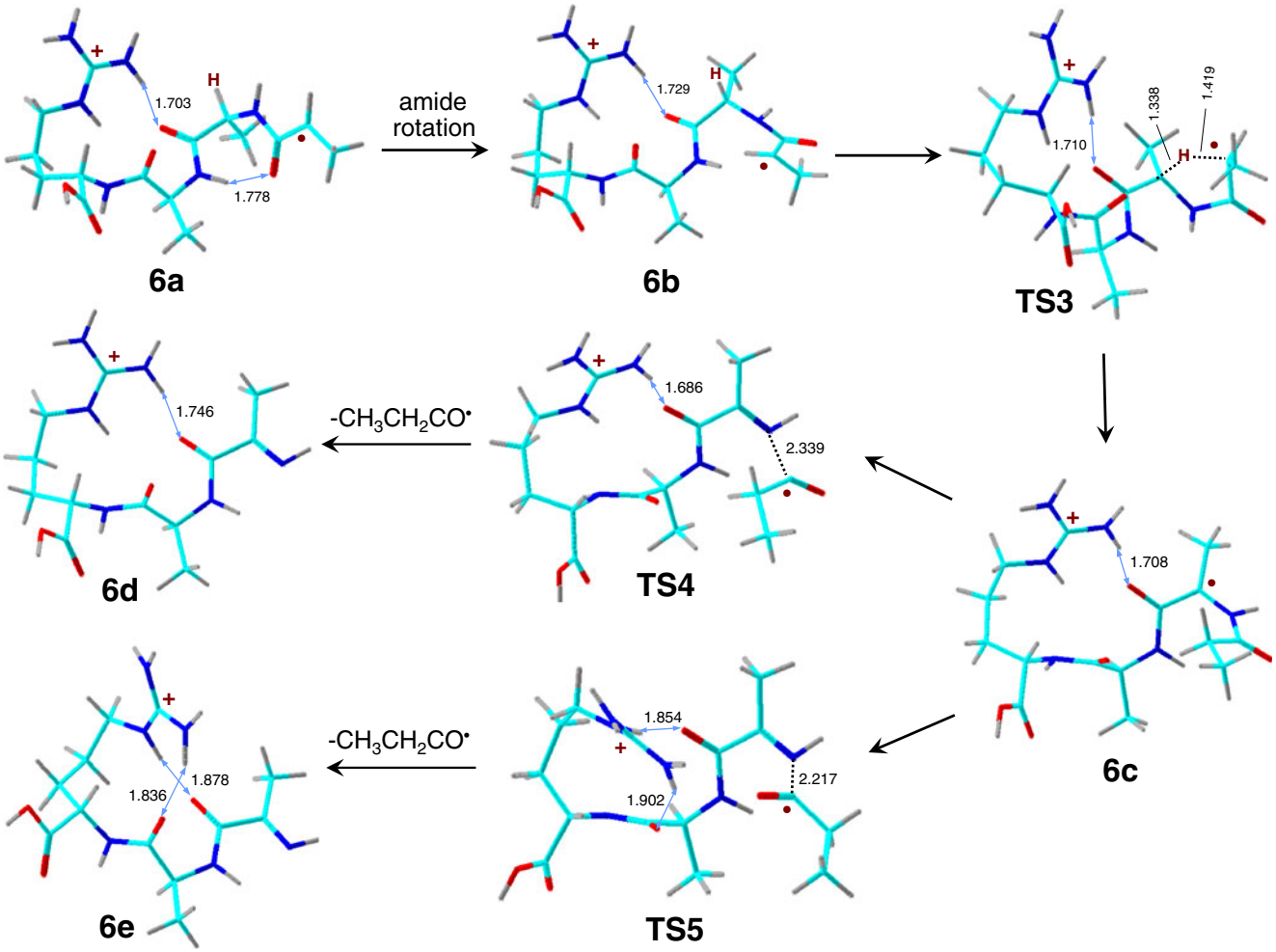

Scheme **6.** Dissociations of z_4 ions from pSAAAR

then can be written in a simplified form (Equation 2 [23]) where σ is the cross section for electron transfer given in Å^2 (10^{-16} cm^2).

$$\Delta E(eV) \cong RE_v(ion) - IE(Cs) - \frac{25.52}{\sqrt{\sigma}} \qquad (2)$$

The calculated RE_v(ion) of the phosphopeptide ions for the formation of cation-radicals in their lowest electronic states are in the 4.3–4.8 eV range, indicating that thermoneutral electron transfer, ΔE=0 eV, would occur at cross sections of 790-3800 Å^2. Smaller cross sections would be endoergic and require inelastic collisions where a small fraction of the center-of-mass kinetic energy (E_{CM}= 19.3 keV) was converted to the internal energy of the charge-reduced ion to make up for the energy deficit. Under these conditions, most collisions are expected to result in very low excitation in the charge-reduced ions which should be formed in low electronic states, such as those calculated for (**1a**$^{+\bullet}$)*. The high density of such low-energy states, >10 states within a 1 eV energy interval, should favor their formation. Regarding dissociations, loss of ammonia on ECID has been shown by ^{15}N labeling to occur from the N-terminal ammonium group [38] and calculated to require very low activation energies when proceeding from the ground electronic state of the charge-reduced ion [53]. This

Table 3. Relative and dissociation energies of non-phosphorylated z_4 fragment ions from pSAAAR

	Relative energy[a,b]			
	B3LYP	B3LYP	PMP2	B3-PMP2[c]
Ion or reaction	6-31+G(d,p)	6-311++G(2d,p)		
6a	0	0	0	0
6b	37	38	33	35
6c	–1	–2	–4	–3
TS3	104	105	96	101
TS4	120	114	138	126
TS5	96	92	108	100
6d+$CH_3CH_2CO^\bullet$	111	104	124	114
6e+$CH_3CH_2CO^\bullet$	96	91	108	100
6f+**6g**	139	131	169	150

[a]In units of kJ mol^{-1}.
[b]Including B3LYP/6-31+G(d,p) zero-point energy corrections and referring to 0 K.
[c]E[B3-PMP2]=0.5{E[B3LYP/6-311++G(2d,p)]+E[PMP2/6-311++G(2d,p)]}.

is corroborated by the present calculations that indicate a spontaneous dissociation of the N-terminal ammonium group in the ground electronic state of a conformer of the charge reduced ion, forming an ion-molecule complex ($\mathbf{3c}^{+\bullet}$, Scheme 3). Thus, our interpretation of the formation of low-energy states upon collisional electron transfer from Cs atoms is consistent with the abundant loss of ammonia in the ECID spectra. It should be noted that inelastic collisions occurring at much smaller cross sections can also result in the formation of excited electronic states in the charge-reduced species and trigger highly endothermic dissociations of strong bonds, as reported previously for several systems [63]. Such dissociations also appear in the ECID spectra and give rise to numerous low-intensity peaks which are mostly unassigned (Figure 1).

The energetics of electron transfer from an anionic donor occurring in slow ion-ion collisions in an ion trap can be described by an energy balance equation (Equation 3 [23]),

$$\Delta E(eV) = RE_a(ion) - [EA(anion) + \Delta E_{exc}(neutral)] \quad (3)$$

which contains the ion adiabatic recombination energy, RE_a(ion), the anion electron binding energy, which is equal to the electron affinity of the corresponding neutral molecule, EA(anion), and the excitation energy of the neutral molecule formed from the anion electron donor, ΔE_{exc}(neutral). Considering the RE_a(ion) values for the phosphopeptides (4.5–4.9 eV) in combination with the literature data for fluoranthene, EA=0.63 eV [64], and ΔE_{exc}(neutral)= 3.06, 3.45, 3.83, and 4.32 eV for the S_1–S_4 states [65], one obtains charge-reduced ion excitation energies with a *bimodal distribution*. Formation of the S_0 state of fluoranthene gives ion excitation energies of 3.9-4.3 eV. Formation of fluoranthene in one of the excited electronic states gives ion excitation energies of $\Delta E \leq 1.3$ eV. It should be noted that the relative cross sections for these processes are unknown. The estimated excitation energies indicate an initial formation of a range of electronic states in charge reduced ions. Those from the highly exothermic electron transfer (ΔE= 3.9–4.3 eV) can correspond to molecular Rydberg states, as discussed below. The electronic states accessed by low-energy ($\Delta E \leq 1.3$ eV) electron transfer from fluoranthene anion-radical are expected to be analogous to those accessed upon collisional electron transfer from Cs. Both types of excitation are sufficient to drive backbone N–C_α bond cleavages which require transition state energies of typically <60 kJ mol^{-1} (0.6 eV) [20]. Note that this range of internal energies can be supplied by exothermic isomerizations of charge-reduced ions to their aminoketyl tautomers ($\mathbf{1a}^{+\bullet}$, $\mathbf{1b}^{+\bullet}$, $\mathbf{3a}^{+\bullet}$, $\mathbf{3b}^{+\bullet}$, $\mathbf{4a}^{+\bullet}$, $\mathbf{4b}^{+\bullet}$, and $\mathbf{4c}^{+\bullet}$) that alone provide 0.9–1.4 eV vibrational excitation to be added to the precursor ion thermal enthalpies (0.95 eV at 298 K).

Differences Between ETD and ECD

The distinct dissociations induced by capture of a free electron indicate that the electronic states involved in this process may differ from those accessed by electron transfer. The primary dissociations triggered by electron capture involve a major loss of an H-atom and cleavages of N–C_α bonds near the arginine residue. Fragments by loss of ammonia (*m/z* 539) and subsequent elimination of phosphoric acid (*m/z* 441) are not observed at all. However, the *m/z* 442 ion from ECD of pSAAAR (measured *m/z* 442.2423, calculated *m/z* 442.2414) corresponds to a combined elimination of NH_3 and H_2PO_4 from the charge-reduced ion. One obvious difference between the ECD and ETD processes is their energetics, as the full recombination energy is deposited in the charge-reduced ion upon electron capture to drive its primary dissociations as well as consecutive dissociations of the primary fragments. Multiple consecutive dissociations are indeed observed in the ECD spectra. These comprise eliminations of H_3PO_4, H_2PO_4, and other dissociations of z ions whose products match those from ETD-CID-MS^3 spectra, e.g., *m/z* 87 from $\boldsymbol{z_1}$, *m/z* 186 and 100 from $\boldsymbol{z_2}$, and *m/z* 283, 256, 244, 200, and 100 from $\boldsymbol{z_3}$. Thus, energy effects can account for some of the differences. For example, the favored secondary elimination of H_2PO_4 on ECD, as opposed to elimination of H_3PO_4, is consistent with the dissociation dynamics of highly energetic ions where the departing H_2PO_4 radical attains kinetic energy that prevents it from engaging in the H transfer reaction (Scheme 5).

A dominant loss of H has been observed previously for ECD of other series of peptide ions [23, 66] and interpreted by the formation of specific electronic states in charge-reduced ions [23]. With the present phosphopeptides, the presumed sites of H loss are the N-terminal ammonium and guanidinium groups, which both are known to lose H atoms upon one-electron reduction [52, 53]. The obvious questions are: (1) Which electronic states are involved? and (2) How are they accessed upon electron capture? Loss of H from neutral primary ammonium groups in ammonium radicals is facile in the ground electronic states, where it is thermoneutral to mildly exothermic and has low TS energies (15–24 kJ mol^{-1})[67–69]. This is due to the nature of the ground-state electronic structure which places the unpaired electron in a symmetry adjusted Rydberg 3s ammonium orbital and weakens the N–H bonds [67, 68]. However, the ground and other low electronic states of the phosphopeptide cation-radicals cannot be described as ammonium 3s Rydberg states. The ammonium group is hydrogen bonded to an amide carbonyl at a 2.5-2.9 Å N…O = C distance, and the Coulomb effect of the charged group substantially lowers the energy of the amide π* state. This results in a substantial mixing of the ammonium 3s and amide π* orbitals in the cation-radicals, as found for the ground and low-lying electronic states in all our phosphopeptide cation-radicals (cf. Figure S4, Supplementary Material). In contrast, several low-lying electronic states were found in peptide cation-radicals that have high electron density in the guanidinium group, as characterized by molecular orbitals, which by their nodality corresponded to σ* or π* states. The σ* states, in

particular, can undergo N–H bond dissociation, whereas the π* states can be expected to promote N–C bond break and loss of guanidine [70]. Hence we conclude that the states responsible for the loss of H atoms upon ECD have high electron density in the guanidinium group.

Electronic States and Dipolar Field Effects

The question of which states are accessed upon electron attachment has been recently addressed by Simons and coworkers [71–73], who presented a semiquantitative model of intramolecular electron transfer according to Landau-Zenner theory. Their model was built on an interaction of ammonium Rydberg 3s and higher ns orbitals with a σ* orbital of a remote disulfide bond or a π* orbital of a remote amide group. According to the analysis of the spatial extent of ammonium 3s, 4s and 5s orbitals, Simons and coworkers estimated the ranges of best overlap of the Rydberg and amide π* orbitals and used them as a measure of the coupling H_{12} terms for electron hopping between the pertinent potential energy surfaces [71]. We now attempt to apply this analysis to ion $\mathbf{2a}^{2+}$, which has an extended structure that separates the amide groups in space and also with regard to their distance from the N-terminal ammonium. Thus, the Ala_1, $pSer_2$, Ala_3, and Ala_4 amide carbonyls in $\mathbf{2a}^{2+}$ are at 2.7, 5.7, 9.2, and 13.4 Å from the ammonium nitrogen atom, which is the center of the putative ns Rydberg orbitals. The Simons model predicts the most favorable overlap zones for ammonium 3s, 4s, and 5s Rydbergs at 4.5–6.6, 7.9–11.1, and 12.3–16.7 Å, respectively. These fit the $pSer_2$, Ala_3, and Ala_4 amide carbonyls but not the Ala_1. The Simons model then explicitly states that amide groups that are too close to the ammonium will not be accessed efficiently, because they lie in the "hollow" region of the 3s wave function. However, the ETD, ECID, and ECD spectra of $\mathbf{2a}^{2+}$ do show abundant z_4 ions (or products of their further dissociations) whose formation is predicted to be "forbidden" by the Simons model. The same holds for the z_4 ion formation in the ETD and ECD spectra of $\mathbf{1a}^{2+}$, $\mathbf{3a}^{2+}$, and $\mathbf{4a}^{2+}$, which occurs in spite of the fact that the pertinent amide groups are in the "forbidden" zone of the Simons model.

It is obvious that it is difficult to apply this model to peptide cation-radicals in which the ammonium groups are as a rule H-bonded to amide or carboxylate carbonyls, resulting in a strong interaction by Coulomb effects and 3s-π* orbital mixing. In our peptides in particular, we do not find ammonium Rydberg 3s or 4s orbitals among the lowest 20 electronic states. This result was independent of whether or not we performed the computational analysis by adding to the 6-311++G(2d,p) basis set another set of special diffuse ns, and np Rydberg-like atomic orbitals [74] on all nitrogen atoms. Rather, we found some of the higher electronic states to have a 3p Rydberg-like character according to their nodality, but those were not centered at the ammonium group. There is no simple model to predict electron transfer from these higher states to the σ* states believed to lead to the loss of guanidinium H atoms.

We have proposed an interpretation of the peculiar ECD behavior of small peptides that was based on the effect of a dipolar field of the peptide ion [23]. The peptide ion dipole was shown to create a 0.4–0.5 V slant in the electrostatic field at distances of 15–20 Å from the center of the ion, which can deform the Rydberg orbitals and steer the incoming electron towards regions of higher positive charge density. This is analogous to electron binding to a neutral molecular dipole that was analyzed by Jordan and Luken [75]. However, there is a difference between the ion and neutral dipoles in that electron binding in the ions is primarily due to the strong Coulomb interaction whereas the dipolar field represents an anisotropic perturbation that affects the electron density distribution.

To further assess the dipole effects on outer molecular wave functions, we performed a simple modeling of the well-studied methylammonium radical [49, 67, 69], in which we inserted a 10-D dipole consisting of ±0.208 atomic point charges that were placed along the C–N axis 10 Å apart and symmetrically positioned with respect of the C and N atoms. According to the wave function analysis (Figure S5), dipole moments of this magnitude (10 D) were able deform the 3s, 4s, 3p and 4p symmetry-adjusted molecular Rydberg orbitals by squeezing, extending, or tilting them along the C–N axis depending on the dipole orientation. Also affected were the excited state energies according to TD-DFT calculations with the 6-311++(+)(2df,2p) basis set where (+) denotes a set of additional very diffuse functions on the N atom according to Simons and coworkers [74]. We presume that similar effects operate in free electron attachment to peptide dications where the outer molecular orbitals of a symmetry-adjusted ns or np Rydberg type, but not necessarily centered at ammonium groups, are distorted by the ion dipolar field. The present phosphopeptide dications all have large dipole moments that were calculated as 11.1, 10.4, 9.3, and 11.5 D for $\mathbf{1a}^{2+}$–$\mathbf{4a}^{2+}$, respectively, which are aligned along the axis connecting the phosphate P and guanidinium C atoms, with the positive end at the guanidinium group. Hence, the dipolar field can increase the density of the outer Rydberg orbitals in the regions of space close to the positive end of the dipole and thus facilitate electron transfer to valence molecular orbitals of the guanidinium group to trigger dissociation by H atom loss [52].

Dipole-guided orientation effects are absent in collisions of fast (keV) peptide ions with Cs atoms, which occur at random orientations [76]. The similarity of dissociations observed under ECID and ETD conditions further suggests that dipole-guided effects are also less important in electron transfer from molecular anion donors. Such a lesser effect is understandable, because (1) the force needed to reorient the fluoranthene anion towards the peptide ion dipole is proportional to its mass which is 3.7×10^5-fold greater than that of an electron, and (2) the reorientation is hampered by the

rotational energy of the orbiting complex which is proportional to its reduced mass.

Conclusions

Electron transfer from neutral and molecular anion electron donors to doubly charged phosphopentapeptides induces cleavages of all peptide N–C_α bonds in addition to loss of ammonia and H atoms. This contrasts dissociations induced by capture of a free electron that result in dominant loss of H atoms followed by elimination of phosphoric acid. We interpret the unusual ECD results by dipole-guided capture of free electrons in the guanidinium group of the arginine residue, triggering H-atom loss. Backbone z fragment ions produced by both ECD and ETD that are terminated by radical phosphoserine residues undergo competitive elimination of phosphoric acid and loss of H_2PO_4 radicals that proceed through common ion neutral complexes as intermediates.

Acknowledgments

The authors gratefully acknowledge support of this research by the National Science Foundation (grants CHE-0750048 for experiments and CHE-0342956 for computations). The Department of Chemistry Computational Center has been supported jointly by the NSF and University of Washington. Thanks are also due to Dr. Priska von Haller and the University of Washington Proteomics Mass Spectrometry Resource for providing access to and assistance with the LTQ-ETD and LTQ-FT-ICR mass spectrometers. S.B.N. thanks Lundbeckfonden for support.

References

1. Zubarev, R.A., Horn, D.M., Fridriksson, E.K., Kelleher, N.L., Kruger, N.A., Lewis, M.A., Carpenter, B.K., McLafferty, F.W.: Electron capture dissociation for structural characterization of multiply charged protein cations. *Anal. Chem.* **72**, 563–573 (2000)
2. Syka, J.E.P., Coon, J.J., Schroeder, M.J., Shabanowitz, J., Hunt, D.F.: Peptide and protein sequence analysis by electron transfer dissociation mass spectrometry. *Proc. Natl. Acad. Sci. U. S. A.* **101**, 9528–9533 (2004)
3. Coon, J.J., Ueberheide, B., Syka, J.E.P., Dryhurst, D.D., Ausio, J., Shabanowitz, J., Hunt, D.F.: Protein identification using sequential ion/ion reactions and tandem mass spectrometry. *Proc. Natl. Acad. Sci. U. S. A.* **102**, 9463–9468 (2005)
4. Stensballe, A., Jensen, O.N., Olsen, J.V., Haselmann, K.F., Zubarev, R. A.: Electron capture dissociation of singly and multiply phosphorylated peptides. *Rapid Commun. Mass Spectrom.* **14**, 1793–1800 (2000)
5. Sweet, S.M.M., Creese, A.J., Cooper, H.J.: Strategy for the identification of sites of phosphorylation in proteins: neutral loss triggered electron capture dissociation. *Anal. Chem.* **78**, 7563–7569 (2006)
6. Kocher, T., Savitski, M.M., Nielsen, M.L., Zubarev, R.A.J.: *Proteome Res.* **5**, 659–668 (2006)
7. Kweon, H.K., Hakansson, K.: Metal oxide-based enrichment combined with gas-phase ion-electron reactions for improved mass spectrometric characterization of protein phosphorylation. *J. Proteome Res.* **7**, 749–755 (2008)
8. Molina, H., Horn, D.M., Tang, N., Mathivanan, S., Pandey, A.: Global proteomic profiling of phosphopeptides using electron transfer dissociation tandem mass spectrometry. *Proc. Natl Acad. Sci. USA* **104**, 2199–2204 (2007)
9. Wiesner, J., Premsler, T., Sickmann, A.: Application of Electron Transfer Dissociation (ETD) for the analysis of post-translational modifications. *Proteomics* **8**, 4466–4483 (2008)
10. Molina, H., Matthiesen, R., Kandasamy, K., Pandey, A.: Comprehensive comparison of collision induced dissociation and electron transfer dissociation. *Anal. Chem.* **80**, 4825–4835 (2008)
11. Mohammed, S., Lorenzen, K., Kerkhoven, R., van Breukelen, B., Vannini, A., Cramer, P., Heck, A.J.R.: Multiplexed proteomics mapping of yeast RNA polymerase II and III allows near-complete sequence coverage and reveals several novel phosphorylation sites. *Anal. Chem.* **80**, 3584–3592 (2008)
12. Sweet, S.M.M., Bailey, C.M., Cunningham, D.L., Heath, J.K., Cooper, H.J.: Large-scale localization of protein phosphorylation by use of electron capture dissociation mass spectrometry. *Mol. Cell. Proteom.* **8**, 904–912 (2009)
13. Kelleher, R.L., Zubarev, R.A., Bush, K., Furie, B., Furie, B.C., McLafferty, F.W., Walsh, C.T.: Localization of labile posttranslational modifications by electron capture dissociation: the case of γ-carboxyglutamic acid. *Anal. Chem.* **71**, 4250–4253 (1999)
14. Mirgorodskaya, E., Roepstorff, P., Zubarev, R.A.: Localization of O-glycosylation sites in peptides by electron capture dissociation in a fourier transform mass spectrometer. *Anal. Chem.* **71**, 4431–4436 (1999)
15. Shi, S.-D.H., Hemling, M.E., Carr, S.A., Horn, D.M., Lindh, I., McLafferty, F.W.: Localization of O-glycosylation sites in peptides by electron capture dissociation in a fourier transform mass spectrometer. *Anal. Chem.* **73**, 19–22 (2001)
16. Creese, A.J., Cooper, H.J.: The effect of phosphorylation on the electron capture dissociation of peptide ions. *J. Am. Soc. Mass Spectrom.* **19**, 1263–1274 (2008)
17. Hayakawa, S., Hashimoto, M., Nagao, H., Awazu, K., Toyoda, M., Ichihara, T., Shigeri, Y.: Study of the dissociation of a charge-reduced phosphopeptide formed by electron transfer from an alkali metal target. Rapid Commun. *Mass Spectrom.* **22**, 567–572 (2008)
18. Hayakawa, S., Matsumoto, S., Hashimoto, M., Iwamoto, K., Nagao, H., Toyoda, M., Shigeri, Y., Tajiri, M., Wada, Y.: High-Energy Electron Transfer Dissociation (HE-ETD) using alkali metal targets for sequence analysis of post-translational peptides. *J. Am. Soc. Mass Spectrom.* **21**, 1482–1489 (2010)
19. Tureček, F.: N–C_α bond dissociation energies and kinetics in amide and peptide radicals. Is the dissociation a non-ergodic process? *J. Am. Chem. Soc.* **125**, 5954–5963 (2003)
20. Chung, T.W., Tureček, F.: Proper and improper aminoketyl radicals in electron-based peptide dissociations. *Int. J. Mass Spectrom.* **2011**, doi:10.1016/j.ijms.2010.06.025
21. Tureček, F., Gu, M., Hop, C.E.C.A.: Franck-condon dominated chemistry. Formation and dissociations of tetrahydroxyphosphoranyl radicals following femtosecond reduction of their cations in the gas phase. *J. Phys. Chem.* **99**, 2278–2291 (1995)
22. Coon, J.J., Syka, J.E.P., Schwartz, J.C., Shabanowitz, J., Hunt, D. F.: Anion dependence in the partitioning between proton and electron transfer in ion/ion reactions. *Int. J. Mass Spectrom.* **236**, 33–42 (2004)
23. Tureček, F., Chung, T.W., Moss, C.L., Wyer, J.A., Ehlerding, A., Zettergren, H., Nielsen, S.B., Hvelplund, P., Chamot-Rooke, J., Bythell, B., Paizs, B.: The histidine effect. Electron transfer and capture cause different dissociations and rearrangements of histidine peptide cation-radicals. *J. Am. Chem. Soc.* **132**, 10728–10740 (2010)
24. Boltalina, O.V., Hvelplund, P., Jørgensen, T.J.D., Larsen, M.C., Larsson, M.O., Sharoitchenko, D.A., Sørensen, M.: Electron capture by fluorinated fullerene anions in collisions with Xe atoms. *Phys. Rev. A* **62**, 023202 (2000)
25. Phillips, J.C., Braun, R., Wang, W., Gumbart, J., Tajkhorshid, E., Villa, E., Chipot, C., Skeel, R.D., Kale, L., Schulten, K.: Scalable molecular dynamics with NAMD. *J. Comp. Chem.* **26**, 1781–1802 (2005)
26. Frisch, M.J., Trucks, G.W., Schlegel, H.B., Scuseria, G.E., Robb, M.A., Cheeseman, J.R., Scalmani, G., Barone, V., Mennucci, B., Petersson, G. A., Nakatsuji, H., Caricato, M., Li, X., Hratchian, H.P., Izmaylov, A.F., Bloino, J., Zheng, G., Sonnenberg, J.L., Hada, M., Ehara, M., Toyota, K., Fukuda, R., Hasegawa, J., Ishida, M., Nakajima, T., Honda, Y., Kitao, O., Nakai, H., Vreven, T., Montgomery Jr., J.A., Peralta, J.E., Ogliaro, F., Bearpark, M., Heyd, J.J., Brothers, E., Kudin, K.N., Staroverov, V.N., Kobayashi, R., Normand, J., Raghavachari, K.,

Rendell, A., Burant, J.C., Iyengar, S.S., Tomasi, J., Cossi, M., Rega, N., Millam, J.M., Klene, M., Knox, J.E., Cross, J.B., Bakken, V., Adamo, C., Jaramillo, J., Gomperts, R., Stratmann, R.E., Yazyev, O., Austin, A. J., Cammi, R., Pomelli, C., Ochterski, J.W., Martin, R.L., Morokuma, K., Zakrzewski, V.G., Voth, G.A., Salvador, P., Dannenberg, J.J., Dapprich, S., Daniels, A.D., Farkas, O., Foresman, J.B., Ortiz, J.V., Cioslowski, J., Fox, D.J.: Gaussian 09, Revision A. 02. Gaussian Inc, Wallingford CT (2009)

27. Homeyer, N., Horn, A.H.C., Lanig, H., Sticht, H.: AMBER force-field parameters for phosphorylated amino acids in different protonation states: phosphoserine, phosphothreonine, phosphotyrosine, and phosphohistidine. *J. Mol. Model.* **12**, 281–289 (2006)
28. MacKerell Jr., A.D., Bashford, D., Bellott, M., Dunbrack Jr., R.L., Evanseck, J.D., Field, M.J., Fischer, S., Gao, J., Guo, H., Ha, S., Joseph-McCarthy, D., Kuchnir, L., Kuczera, K., Lau, F.T.K., Mattos, C., Michnick, S., Ngo, T., Nguyen, D.T., Prodhom, B., Reiher III, W. E., Roux, B., Schlenkrich, M., Smith, J.C., Stote, R., Straub, J., Watanabe, M., Wiorkiewicz-Kuczera, J., Yin, D., Karplus, M.: All-atom empirical potential for molecular modeling and dynamics studies of proteins. *J. Phys. Chem.* B **102**, 3586–3616 (1998)
29. Sugita, Y., Okamoto, Y.: Replica-exchange molecular dynamics method for protein folding. *Chem. Phys. Lett.* **314**, 141–151 (1999)
30. Stewart, J.J.P.: Optimization of parameters for semiempirical methods. V. Modification of NDDO approximations and application to 70 elements. *J. Mol. Model.* **13**, 1173–1213 (2007)
31. Becke, A.D.: New mixing of hartree-fock and local density-functional theories. *J. Chem. Phys.* **98**, 1372–1377 (1993)
32. Becke, A.D.: Density functional thermochemistry. III. The role of exact exchange. *J. Chem. Phys.* **98**, 5648–5652 (1993)
33. Stephens, P.J., Devlin, F.J., Chabalowski, C.F., Frisch, M.J.: Ab initio calculation of vibrational absorption and circular dichroism spectra using density functional force fields. *J. Phys. Chem.* **98**, 11623–11627 (1994)
34. Møller, C., Plesset, M.S.: A note on an approximation treatment for many-electron systems. *Phys. Rev.* **46**, 618–622 (1934)
35. Tureček, F.: Proton affinity of dimethyl sulfoxide and relative stabilities of C_2H_6OS molecules and $C_2H_7OS^+$ ions. A comparative G2(MP2) Ab initio and density functional theory study. *J. Phys. Chem.* A **102**, 4703–4713 (1998)
36. Furche, F., Ahlrichs, R.: Adiabatic time-dependent density functional methods for excited state properties. *J. Chem. Phys.* **117**, 7433–7447 (2002)
37. Hayakawa, S., Matsubara, H., Panja, S., Hvelplund, P., Nielsen, S.B., Chen, X., Tureček, F.: Experimental evidence for an inverse hydrogen migration in arginine radicals. *J. Am. Chem. Soc.* **130**, 7645–7654 (2008)
38. Holm, A.I.S., Hvelplund, P., Kadhane, U., Larsen, M.K., Liu, B., Nielsen, S.B., Panja, S., Pedersen, J.M., Skrydstrup, T., Støchkel, K., Williams, E.R., Worm, E.S.: On the mechanism of electron-capture-induced dissociation of peptide dications from ^{15}N-labeling and crown-ether complexation. *J. Phys. Chem.* A **111**, 9641–9643 (2007)
39. Han, H., Xia, Y., McLuckey, S.A.: Ion trap collisional activation of c and $z^{\bullet}$ ions formed via gas-phase ion/ion electron transfer dissociation. *J. Proteome Res.* **6**, 3062–3069 (2007)
40. Tureček, F., Syrstad, E.A.: Mechanism and energetics of intramolecular hydrogen transfer atom transfer in amide and peptide radicals and cation-radicals. *J. Am. Chem. Soc.* **125**, 3353–3369 (2003)
41. Chung, T.W., Tureček, F.: Backbone and side-chain specific dissociations of z ions from nontryptic peptides. *J. Am. Soc. Mass Spectrom.* **21**, 1279–1295 (2010)
42. Moore, B.N., Blanksby, S.J., Julian, R.R.: Ion-molecule reactions reveal facile radical migration in peptides. *Chem. Commun.* **33**, 5015–5017 (2009)
43. Ly, T., Julian, R.R.: Tracking radical migration in large hydrogen deficient peptides with covalent labels: facile movement does not equal indiscriminate fragmentation. *J. Am. Soc. Mass Spectrom.* **20**, 1148–1158 (2009)
44. Sun, Q., Nelson, H., Ly, T., Stoltz, B.M., Julian, R.R.: Side chain chemistry mediates backbone fragmentation in hydrogen deficient peptide radicals. *J. Proteome Res.* **8**, 958–966 (2009)
45. Diedrich, J.K., Julian, R.R.: Site-specific radical directed dissociation of peptides at phosphorylated residues. *J. Am. Chem. Soc.* **130**, 12212–12213 (2008)
46. Schug, K., Lindner, W.: Development of a screening technique for noncovalent complex formation between guanidinium- and phosphate-functionalized amino acids by electrospray ionization ion trap mass spectrometry: assessing ionization and functional group interaction. Int. *J. Mass Spectrom.* **235**, 213–222 (2004)
47. Woods, A.S., Ferre, S.: Amazing stability of the arginine-phosphate electrostatic interaction. *J. Proteome Res.* **4**, 1397–1402 (2005)
48. Jackson, S.N., Moyer, S.C., Woods, A.S.: The role of phosphorylated residues in peptide-peptide noncovalent complexes formation. *J. Am. Soc. Mass Spectrom.* **19**, 1535–1541 (2008)
49. Syrstad, E.A., Tureček, F.: Toward a general mechanism of electron-capture dissociation. *J. Am. Soc. Mass Spectrom.* **16**, 208–224 (2005)
50. Sobczyk, M., Anusiewicz, I., Berdys-Kochanska, J., Sawicka, A., Skurski, P., Simons, J.: Coulomb-assisted dissociative electron attachment: application to a model peptide. *J. Phys. Chem. A* **109**, 250–258 (2005)
51. Anusiewicz, I., Berdys-Kochanska, J., Simons, J.: Electron attachment step in Electron Capture Dissociation (ECD) and Electron Transfer Dissociation (ETD). *J. Phys. Chem. A* **109**, 5801–5813 (2005)
52. Hao, C., Seymour, J.L., Tureček, F.: Electron super-rich radicals in the gas phase. A neutralization-reionization mass spectrometric and Ab Initio/RRKM study of diaminohydroxymethyl and triaminomethyl radicals. *J. Phys. Chem. A* **111**, 8829–8843 (2007)
53. Tureček, F., Chen, X., Hao, C.: Where does the electron go? electron distribution and reactivity of peptide cation-radicals formed by electron transfer in the gas phase. *J. Am. Chem. Soc.* **130**, 8818–8833 (2008)
54. DeGnore, J.P., Qin, J.: Fragmentation of phosphopeptides in an ion trap mass spectrometer. *J. Am. Soc. Mass Spectrom.* **9**, 1175–1188 (1998)
55. Tholey, A., Reed, J., Lehmann, W.D.: Electrospray tandem mass spectrometric studies of phosphopeptides and phosphopeptide analogues. *J. Mass Spectrom.* **34**, 117–123 (1999)
56. Reid, G.E., Simpson, R.J., O'Hair, R.A.J.: Leaving group and gas phase neighboring group effects in the side chain losses from protonated serine and its derivatives. *J. Am. Soc. Mass Spectrom.* **11**, 1047–1060 (2000)
57. Palumbo, A.M., Tepe, J.J., Reid, G.E.: Mechanistic insights into the multistage gas-phase fragmentation behavior of phosphoserine and phosphothreonine-containing peptides. *J. Proteome Res.* **7**, 771–779 (2008)
58. Boersema, P.J., Mohammed, S., Heck, A.J.R.: Phosphopeptide fragmentation and analysis by mass spectrometry. *J. Mass Spectrom.* **44**, 861–878 (2009)
59. Yu, D., Rauk, A., Armstrong, D.A.: Radicals and ions of glycine: An ab initio study of the structures and gas-phase thermochemistry. *J. Am. Chem. Soc.* **117**, 1789–1796 (1995)
60. Rauk, A., Yu, D., Taylor, J., Shustov, G.V., Block, D.A., Armstrong, D. A.: Effects of structure on α-C–H bond enthalpies of amino acid residues: relevance to H transfers in enzyme mechanisms and in protein oxidation. *Biochemistry* **38**, 9089–9096 (1999)
61. McMillen, D.F., Golden, D.M.: Hydrocarbon bond dissociation energies. *Ann. Rev. Phys. Chem.* **33**, 493–532 (1982)
62. Hayakawa, S., Minami, K., Iwamoto, K., Toyoda, M., Ichihara, T., Nagao, H.: Potential crossing position in electron transfer of a doubly charged ion and an alkali metal target measured using thermometer molecule $W(CO)_6$. *Int. J. Mass Spectrom.* **266**, 122–128 (2007)
63. Holm, A.I.S., Larsen, M.K., Panja, S., Hvelplund, P., Nielsen, S.B., Leib, R.D., Donald, W.A., Williams, E.R., Hao, C., Tureček, F.: Electron capture, femtosecond electron transfer, and theory: a study of noncovalent crown ether 1, *n*-diammonium alkane complexes. *Int. J. Mass Spectrom.* **276**, 116–126 (2008)
64. Maddams, W.F., Schnurmann, R.: Ultraviolet absorption spectrum of fluoranthene. *J. Chem. Phys.* **19**, 973–974 (1951)
65. Michl, J.: Electronic structure of non-alternant hydrocarbons: their analogues and derivatives. XVIII. The electronic spectrum and electron affinity of fluoranthene. *J. Mol. Spectrosc.* **30**, 66–76 (1969)
66. Cooper, H.J.: Investigation of the presence of *b* ions in electron capture dissociation mass spectra. *J. Am. Soc. Mass Spectrom.* **16**, 1932–1940 (2005)
67. Boldyrev, A.I., Simons, J.: Theoretical search for large rydberg molecules: NH_3CH_3, $NH_2(CH_3)_2$, $NH(CH_3)_3$, and $N(CH_3)_4$. *J. Chem. Phys.* **97**, 6621–6627 (1992)
68. Shaffer, S.A., Tureček, F.: Hydrogentrimethylammonium. A marginally stable hypervalent radical. *J. Am. Chem. Soc.* **116**, 8647–8653 (1994)

69. Yao, C., Tureček, F.: Hypervalent ammonium radicals. Competitive N–C and N–H bond dissociations in Methylammonium and Ethylammonium. *Phys. Chem. Chem. Phys.* **7**, 912–920 (2005)
70. Panja, S., Nielsen, S.B., Hvelplund, P., Tureček, F.: Inverse hydrogen atom migration in arginine-containing peptide ions upon electron transfer. *J. Am. Soc. Mass Spectrom.* **19**, 1726–1742 (2008)
71. Neff, D., Sobczyk, M., Simons, J.: Through-space and through-bond electron transfer within positively charged peptides in the gas phase. *Int. J. Mass Spectrom.* **276**, 91–101 (2008)
72. Simons, J.: Mechanisms for S–S and N–C_α bond cleavage in peptide ECD and ETD mass spectrometry. *Chem. Phys. Lett.* **484**, 81–95 (2010)
73. Simons, J.: Analytical model for rates of electron attachment and intramolecular electron transfer in electron transfer dissociation mass spectrometry. *J. Am. Chem. Soc.* **132**, 7074–7085 (2010)
74. Skurski, P., Gutowski, M., Simons, J.: How to choose a one-electron basis set to reliably describe a dipole-bound state. *Int. J. Quantum Chem.* **80**, 1024–1038 (2000)
75. Jordan, K.D., Luken, W.: Theoretical study of the binding of an electron to a molecular dipole: $LiCl^{-}$*. *J. Chem. Phys*. **64**, 2760–2766 (1976)
76. Turecek, F.: Transient intermediates of chemical reactions by neutralization-reionization mass spectrometry. *Top. Curr. Chem.* **225**, 77–129 (2003)